CrossMark

An Initial Overview of the Extent and Structure of Recent Star Formation within the Serpens Molecular Cloud Using *Gaia* Data Release 2

Gregory J. Herczeg (沈雷歌)[1], Michael A. Kuhn[2], Xingyu Zhou[1,3], Jennifer Hatchell[4], Carlo F. Manara[5],
Doug Johnstone[6,7], Michael Dunham[8], Anupam Bhardwaj[1], Jessy Jose[9], and Zhen Yuan (袁珍)[10]

[1] Kavli Institute for Astronomy and Astrophysics, Peking University, Yiheyuan Lu 5, Haidian Qu, 100871 Beijing, People's Republic of China
[2] Department of Astronomy, California Institute of Technology, Pasadena, CA 91125, USA
[3] Department of Astronomy, Peking University, Yiheyuan 5, Haidian Qu, 100871 Beijing, People's Republic of China
[4] Physics and Astronomy, University of Exeter, Stocker Road, Exeter EX4 4QL, UK
[5] European Southern Observatory, Karl-Schwarzschild-Strasse 2, D-85748 Garching bei München, Germany
[6] NRC Herzberg Astronomy and Astrophysics, 5071 West Saanich Road, Victoria, BC V9E 2E7, Canada
[7] Department of Physics and Astronomy, University of Victoria, Victoria, BC V8P 1A1, Canada
[8] Department of Physics, State University of New York at Fredonia, Fredonia, NY 14063, USA
[9] Indian Institute of Science Education and Research Tirupati, Rami Reddy Nagar, Karakambadi Road, Mangalam (PO) Tirupati 517507, India
[10] Key Laboratory for Research in Galaxies and Cosmology, Shanghai Astronomical Observatory, Chinese Academy of Sciences, 80 Nandan Road, Shanghai 200030, People's Republic of China
Received 2018 December 22; revised 2019 April 8; accepted 2019 April 8; published 2019 June 19

Abstract

The dense clusters within the Serpens Molecular Cloud are among the most active regions of nearby star formation. In this paper, we use *Gaia* DR2 parallaxes and proper motions to statistically measure ∼1167 kinematic members of Serpens, few of which have been previously identified, to evaluate the star formation history of the complex. The optical members of Serpens are concentrated in three distinct groups located at 380–480 pc; the densest clusters are still highly obscured by optically thick dust and have few optical members. The total population of young stars and protostars in Serpens is at least 2000 stars, including past surveys that were most sensitive to protostars and disks, and may be much higher. Distances to dark clouds measured from deficits in star counts are consistent with the distances to the optical star clusters. The Serpens Molecular Cloud is seen in the foreground of the Aquila Rift, dark clouds located at 600–700 pc, and behind patchy extinction, here called the Serpens Cirrus, located at ∼250 pc. Based on the lack of a distributed population of older stars, the star formation rate throughout the Serpens Molecular Cloud increased by at least a factor of 20 within the past ∼5 Myr. The optically bright stars in Serpens Northeast are visible because their natal molecular cloud has been eroded, not because they were flung outwards from a central factory of star formation. The separation between subclusters of 20–100 pc and the absence of an older population together lead to speculation that an external forcing was needed to trigger the active star formation.

Key words: open clusters and associations: general – planetary systems – protoplanetary disks – stars: low-mass – stars: pre-main sequence

Supporting material: machine-readable table

1. Introduction

The spatial distribution of young star clusters provides constraints for theoretical explanations for the growth of molecular clouds and subsequent star formation (e.g., Cunningham et al. 2018; Vázquez-Semadeni et al. 2018). Our descriptions of these star-forming regions are built upon a census of the cloud complexes and stellar population. The Serpens Molecular Cloud, one of the most active sites of ongoing star formation within 500 pc, is particularly challenging for membership analyses because the region is seen against the crowded background of the galactic plane, is visually located against a long swath of extinction, and suffers from historical uncertainties in the distances to the different clouds. The *Gaia* satellite (Gaia Collaboration et al. 2016, 2018) is now revolutionizing the description of star-forming regions. Initial results from *Gaia* DR2 have described the star formation history of the Orion molecular cloud complexes (Kounkel et al. 2018), the expansion of individual young clusters and subclusters (Dzib et al. 2018; Zari et al. 2018; Cantat-Gaudin et al. 2019; Kuhn et al. 2019), the distinction between subgroups within single regions (Beccari

et al. 2018; Roccatagliata et al. 2018), and the memberships of specific regions for analysis of disk fractions (Manara et al. 2018) and older populations (Luhman 2018; Damiani et al. 2019).

In this paper, we apply the power of *Gaia* astrometry to star formation in the Serpens-Aquila complex. This collection of cloud complexes[11] can be subdivided into several distinct clouds and star-forming regions (see the map of *Gaia* DR2 star counts in Figure 1 and extinction maps in Cambrésy 1999 and Green et al. 2015). The Serpens Main star-forming region, located on the northern side of the rift, has historically been the most well studied site of active star formation within the complex (see the review by Eiroa et al. 2008). About 3° to the south of Serpens Main, a separate cloud contains the H II region W40 on its east side and Serpens South ∼30′ to the west. W40,

---

[11] We adopt the following nomenclature for this region: Serpens is the collection of star-forming regions and optically thick molecular clouds at 370–500 pc, located roughly in a rectangle from 276° to 281° in R.A. and from −5° to +2° in decl. The Aquila Rift is the elongated swath of extinction that cuts diagonally across most of our field and is located at 600–700 pc. Serpens Cirrus is a more diffuse cloud to the southwest of Serpens and is located at ∼250 pc.
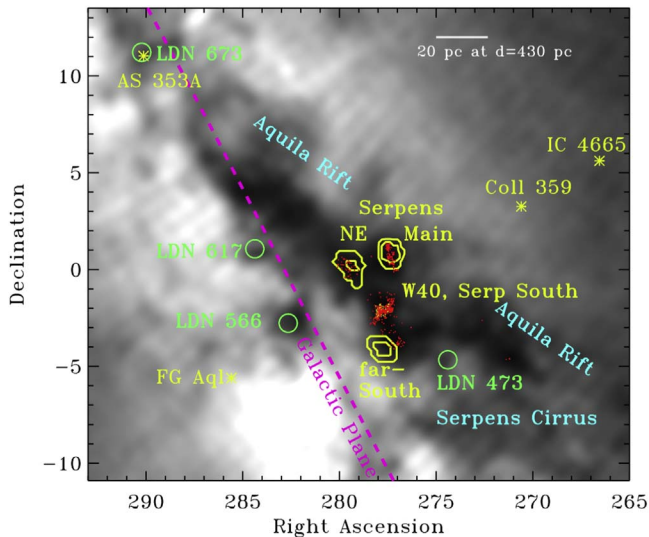
Figure 1. A map of the number of stars with distances 1000–1500 pc, behind the Serpens star-forming regions and the Aquila Rift. The dark regions trace dust extinction, with locations of dust that correlate well with the extinction map from Cambrésy (1999). The prominent star-forming regions Serpens Main and Serpens South are labeled on the map. Several dark clouds are labeled (green circles), including LDN 673 on the northeast end of the Serpens star formation complexes (Lynds 1962; see also Dobashi 2011). The diagonal Aquila Rift cuts across the galactic plane (dashed purple line); the Serpens Cirrus is located in the southwest. Three clusters of optically bright stars in Serpens are identified with yellow contours. The youngest regions, including W40 and Serpens South, are identified on the map by the location of protostars and disks that were identified by Povich et al. (2013; yellow circles) and Dunham et al. (2015; red circles).

discovered in surveys of 22 cm radio continuum emission and Hα emission (Westerhout 1958; Sharpless 1959), includes a compact cluster of ∼500 candidate young stars (Kuhn et al. 2010; Mallick et al. 2013) and is ionized by several OB stars (Smith et al. 1985; Shuping et al. 2012). Serpens South, a dense embedded cluster in a massive molecular filament, was discovered in the *Spitzer* survey of Gutermuth et al. (2008) and is rich in protostars (see also Dunham et al. 2015; Könyves et al. 2015). Some young stars and H II regions are also located in a region around MWC 297 (e.g., Bontemps et al. 2010; Dunham et al. 2015; Rumble et al. 2015), hereafter called Serpens Far-South. A fourth group of the cloud complex, which we designate Serpens Northeast based on its location 1° east of Serpens Main, was found by Dunham et al. (2015) to have its own population of young stars. These groups of young stars are visually interspersed within the Aquila Rift, a set of dark molecular clouds elongated across >25° on the sky (260 pc at a distance of 600 pc).

The physical connection between these complexes has been questioned, in part because the distances to Serpens Main, Serpens South and W40, and the Aquila Rift have been controversial (see discussions in Eiroa et al. 2008; Prato et al. 2008, and Rodney & Reipurth 2008). The VLBI parallax measurements of masers by Ortiz-León et al. (2017) led to (separate) distances of 436 pc to Serpens Main and to W40. The similarity in velocities indicates that the entire region is located at the same distance (see discussion in Ortiz-León et al. 2017). However, a recent analysis of the X-ray luminosity function of Serpens South placed the cluster at 260 pc (Winston et al. 2018), consistent with the previous identification of an extinction wall at ∼250 pc to both Serpens Main and the Aquila Rift (Straižys et al. 1996, 2003). In the 3D structure of

the Milky Way from the velocity analysis of Lallement et al. (2014), the Aquila Rift is also placed at ∼250 pc. The possible connections in the wider complex have also suffered from uneven accounting of stellar membership; many dedicated surveys on smaller regions (e.g., Kuhn et al. 2010; Mallick et al. 2013; Povich et al. 2013; Dunham et al. 2015) miss most optical members of Serpens Northeast and Serpens Far-South that are found in this paper.

With all-sky coverage, *Gaia* DR2 provides a consistent and near-complete, magnitude-limited set of astrometry and photometry over a full field of interest. When compared to past membership studies, our application of *Gaia* DR2 astrometry is particularly sensitive to the lightly absorbed population, including the disk-free (Class III) young stars that are missed in searches based on excess infrared emission. Our search over a wide field of view probes both recent star formation and any population of older stars from past epochs of star formation. In this paper, we use *Gaia* DR2 almost exclusively to identify and analyze the population of young stars in the Serpens star-forming regions and the lack of young stars in the Serpens Cirrus. Distances to different subclusters and to dust-extinction regions confirm the accurate VLBI distance measurements of Ortiz-León et al. (2017) to the Serpens star-forming regions[12] and reveal the presence of some dust at 250 pc that is not actively forming stars. Most of the optically thick dust outside of the active Serpens star-forming regions are located at ∼600–700 pc.

2. Sample and Data

Our analysis in this paper is based primarily on data from *Gaia* DR2. We downloaded all stars in the *Gaia* DR2 archive (Arenou et al. 2018) in a large area around the star formation complexes. We began by downloading 1 deg^2 around both the Serpens Main and W40/Serpens South clusters. Our desire to describe the dust extinction in the context of the broader cloud led us to download the surrounding few square degrees. Several iterations later, we had downloaded all ∼140 million objects in ∼830 deg^2 around Serpens-Aquila, from $\alpha = 262°$ to 294° in R.A. and $\delta = -12°$ to 14° in decl.

The most relevant data are the stellar positions, proper motions, parallaxes, and G-, Bp-, and Rp-band magnitudes, along with the associated errors and the excess astrometric noise (Evans et al. 2018; Lindegren et al. 2018). The optical photometry from *Gaia* is supplemented with 2MASS JHK_S (Cutri et al. 2003). Objects fainter than $G = 19$ mag are not considered in the bulk analysis because the unreliability of small parallaxes of faint objects leads to an artificially large population of stars at <300 pc, even after accounting for the listed errors.[13] Most analyses in this paper are also restricted to stars with excess astrometric noise less than 2 mas and to stars with parallaxes measured to a signal-to-noise greater than 5–20, depending on the analysis. However, fainter stars and stars with parallaxes consistent with 0 are used when evaluating membership of candidates selected from past surveys. The

---

[12] A contemporaneous and independent paper by Ortiz-León et al. (2018) uses *Gaia* DR2 data to confirm the VLBI distances to Serpens Main, Serpens South, and W40, consistent with our results.

[13] The star-count map for all stars with $G < 19$ does not show any evidence for optical extinction until ∼250–400 pc to the Serpens star formation complex; however, for fainter stars, the extinction regions are prominent in density maps of stars with parallaxes >10 mas (<100 pc). The tail of the error distribution in parallaxes leads to a background population that could be interpreted as nearby objects.
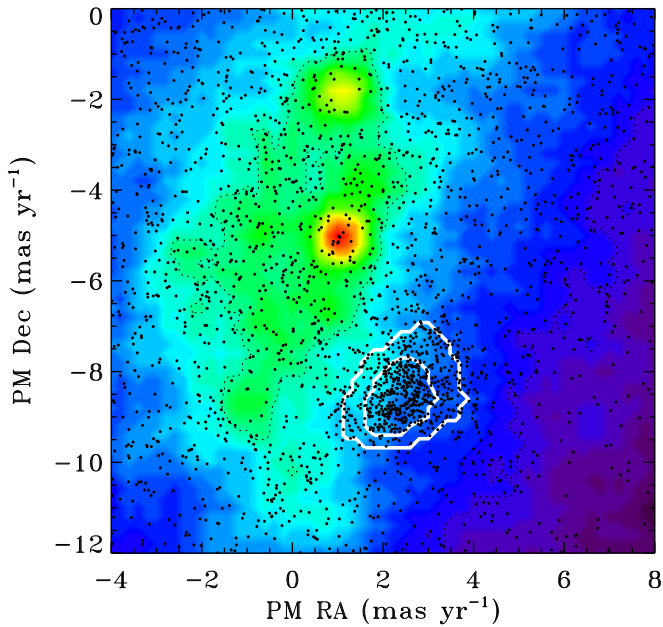
Figure 2. A heat map of the proper motions of all stars in the full downloaded area with distances between 350–500 pc and $\varpi/\sigma(\varpi) > 10$. The proper motion of stars at this distance around the Serpens star-forming region (R.A. of 276–281 and decl. from $-5°$ to $2°$; solid white contours; black dots show individual stars) is offset in proper motion from this field population. For both the Serpens and field samples, contours are shown for 0.2 and 0.5 times the peak number of stars in a 0.2×0.2 (mas/yr)^2 box. The two bright overdensities in the heat map are the older clusters IC 4796 and NGC 6633.

systematic error of $\sim$0.1 mas in *Gaia* DR2 parallax measurements (e.g., Luri et al. 2018; Leung & Bovy 2019) is ignored in our analysis and is applied only in the final measurements of distance.

All star-count maps created from *Gaia* observations in this region include diagonal dips in the number of stars brighter than $G = 19$. These features must be related to some loss in sensitivity or astrometric accuracy, presumably at the edges of the *Gaia* field of view, as *Gaia* scans across the sky. The depth and accuracy also depend on star density, which varies strongly across our field. We ignore these systematic problems.

For ease of reference, at 430 pc, a distance of 1° corresponds to 7.5 pc, while a proper motion of 1 mas yr^{-1} corresponds to 2 km s^{-1}.

3. A Search for Young Stars in Serpens

In this section, we identify several young clusters within our field in a search of the 5D phase space of location, proper motion, and distance. The ability to separate the young stars in the Serpens in both distance and proper motion provides us with the leverage to distinguish the young star population from the field population, without resorting to spectroscopic or even photometric criteria (see, e.g., seminal papers by Blaauw 1956; de Zeeuw et al. 1999). Photometry is not directly used in these selections, beyond the initial *Gaia* selection of targets and our brightness requirement of $G < 19$ mag. However, the stars in these clusters are located above the main sequence in color–magnitude diagrams (see Section 5.2), which reinforces the conclusion that they are young.

Although the density of stars is high toward Serpens, the members of the star-forming regions and young clusters are readily identified in both proper motion and distance. Figure 2 shows the proper motions of all stars in the full field with

distances $\sim$350–500 pc (see Figure 3 for this circular logic) and parallaxes measured to better than $\varpi/\sigma(\varpi) > 10$, for the full field (except Serpens) and for a box around Serpens, between $\alpha = 276°$ to $281°$ in R.A. and $\delta = -5°$ to $2°$ in decl. A clear overdensity of stars is visible at PM(R.A.) $\approx$ 2.5 mas yr^{-1} and PM(decl.) ≈ -8.5 mas yr^{-1}. In this initial analysis, this Serpens box includes 470 stars with proper motions within 1 mas yr^{-1} of the Serpens centroid; the same distribution as the rest of the field would have yielded only 36 stars in the same region. The distribution of parallaxes of stars within this box (Figure 3) shows a large excess at 350–500 pc, the expected distance for the Serpens star-forming region.

This overdensity in proper motion and parallax space corresponds to the optical members of the Serpens star-forming region. Figure 4 shows the spatial distribution of stars between 350–550 pc and with a proper motion within 2 mas yr^{-1} of the centroid proper motion. Three distinct regions stand out: the optical counterparts of Serpens Main and Serpens Northeast, as well as a region associated with MWC 297 and Sh 2-62, here called Serpens Far-South (also sometimes called the MWC 297 group or region; Rumble et al. 2015). The intervening drop in stellar density between Serpens Main and Serpens Northeast does not correspond to any increase in extinction, which demonstrates that the two subclusters are distinct.

The properties of each subcluster are listed in Table 1. The distance, location, and proper motion are first estimated with loose distance and proper motion criteria for a sample of stars with parallax measured to $\varpi/\sigma(\varpi) > 20$. The distance is then refined from parallaxes of a restricted candidate membership criteria, restricted to stars with 2σ (here σ is the scatter in proper motions, not an uncertainty) of the proper motion centroid and within $0°.5$–$0°.8$ of the spatial centroid of the cluster. The proper motion is refined with a similar membership criteria, with a 2σ restriction in distance rather than in proper motion. The final proper motion median and standard deviation are calculated by fitting a Gaussian profile to the proper motion in both R.A. and decl. The final distance measurement is calculated by a weighted average of the parallax, with a statistical uncertainty of 1–2 pc. The listed standard deviation in the distance is the standard deviation in a distance spread that is required to reproduce the observed spread in parallaxes. The distance spread for Serpens Far-South is 2 pc, indicating that the measured distance spread is nearly consistent with the spread expected from only the parallax errors of the members. Other regions have distance spreads that are larger than the projected radius of the cluster, which indicates that either the parallax errors are underestimated, that a population of distributed young stars within Serpens contaminates the subcluster population, or that the subclusters are elongated along our line of sight.

3.1. The Total Optically Bright Population of the Serpens Star-forming Regions

In this subsection, we estimate the total number of stars in our sample that are located within each of the subclusters identified above, as well as the total number of stars within the Serpens star-forming region. These populations are measured by estimating a radial size of the cluster using star counts and subsequently measuring the number of stars from the distribution of proper motions within a circular area (Table 2). The stars are best separated from field stars in the proper motion in decl., so the total number of stars is measured
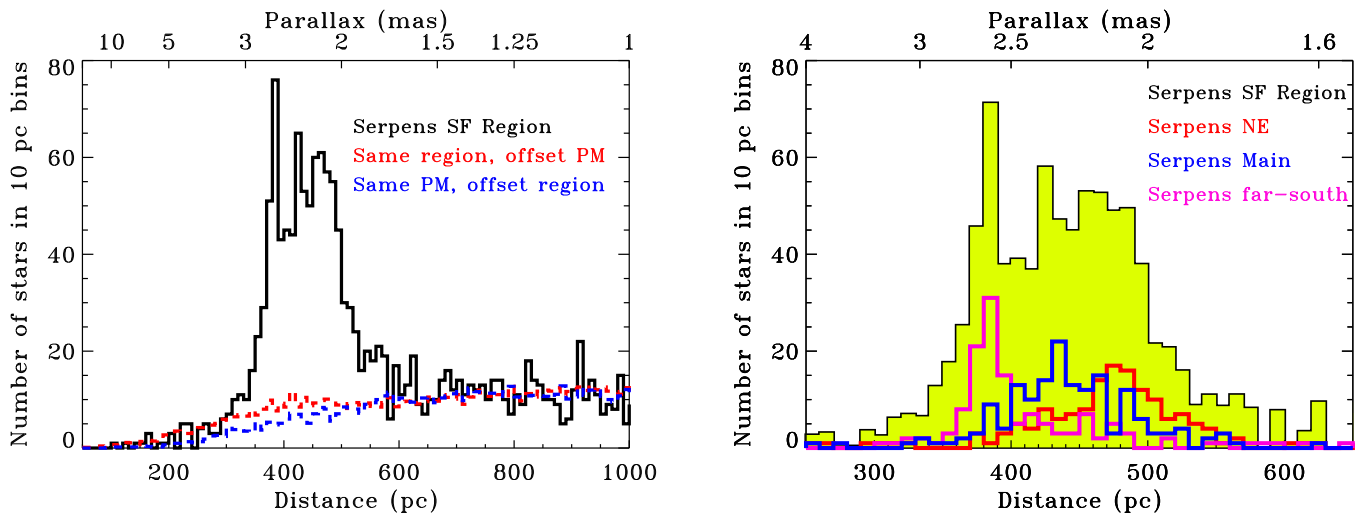
Figure 3. Left: star counts vs. distance for stars with proper motions within 2 mas yr^{-1} of the Serpens star formation centroid (black solid line; see centroid in Figure 2), compared with star counts for the full downloaded area outside of the Serpens star-forming regions (blue dashed line) and to star counts from the Serpens star-forming region but with offset proper motions. The off-cloud and offset proper motion populations are scaled to that of the Serpens star-forming region at 150–300 and 700–900 pc. The excess number of stars from 350 to 500 are the young members. Right: three peaks in the histogram of star counts vs. distance correspond to three different subclusters: Serpens Main, Serpens Northeast, and Serpens Far-South (each restricted to within 1 mas yr^{-1} in proper motion and 1° of the centroid of each subregion; see also Table 1 and Figure 4).
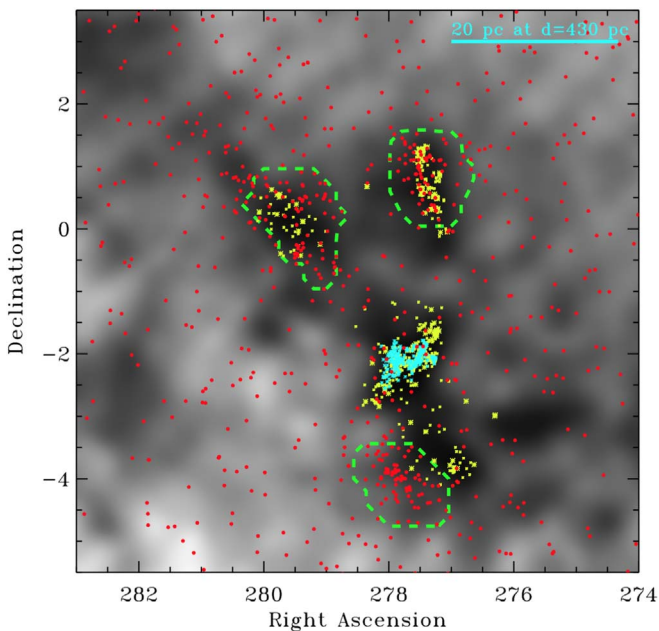

Figure 4. The spatial location of stars with $\varpi/\sigma(\varpi) > 10$, distances between 350–550 pc, and proper motions within 2 mas yr^{-1} of the centroid proper motion of the Serpens star-forming region (red circles), compared with the distribution of Class 0/I/II protostars identified from mid-IR photometry (small yellow asterisks denote disks and large yellow asterisks denote protostars from Dunham et al. 2015; blue asterisks from Povich et al. 2013). The optical members are located in three distinct clusters: Serpens Main, Serpens Northeast, and Serpens Far-South (outlined by the dashed green contours established from stellar densities). Many protostars but few optical counterparts are associated with the optically thick Serpens South and W40 molecular clouds, perhaps indicating that these regions are younger than the other clusters. Field stars are contaminants and are spread roughly equally throughout this region.

by fitting a Gaussian profile to that distribution within some circular area on the sky. Figure 5 shows that the stars extend to ~3°.2 (26 pc) for 90% completeness, from an approximate center of $\alpha = 278°$ and $\delta = -1°.5$. No significant population of young stars is detected between 3.5 and 4°.5 of this location.

A small population of young stars in Serpens is located beyond 4°.5 and is discussed in Section 3.2.

The Serpens star-forming region includes 1167 members (evaluated statistically) with *Gaia* DR2 parallaxes with $\varpi/\sigma (\varpi) > 5$. Roughly 60% of those stars are located within one of the three main optical clusters; a few additional stars are likely members of the W40/Serpens South cluster. The remaining stars are distributed throughout the region. The accounting of optical members likely misses at least half of the full membership, for many reasons. The color–magnitude diagrams (discussed in Section 5) indicate a sensitivity to stars with masses larger than 0.2–0.3 $M_\odot$. The embedded protostars are optically faint and not detectable with *Gaia* (see Section 5.1). Our accounting also misses almost all members of W40 and Serpens South (Mallick et al. 2013; Povich et al. 2013; Dunham et al. 2015), including any diskless population, because they are buried deep in the molecular cloud. Any stars on the back side of dark clouds would also be too faint for *Gaia*.

While the statistical measurement on the number of members is accurate, the membership probability for any individual star depends on the field population. This probability is higher for stars with parallaxes measured with $\varpi/\sigma(\varpi) > 20$ and for those with proper motions and locations near the respective centroids of each cluster. The total population from this specific analysis is accurate to ~5%, with the uncertainty dominated by the uncertainty in defining the region in physical, proper motion, and distance space. The subtraction of field stars does not significantly contribute to these errors. More advanced techniques should eventually be applied to assess membership probabilities and then analyze cluster properties based on those probabilities.

This approach to identifying cluster members excludes any runaway stars that were ejected with proper motions larger than 2 mas yr^{-1} (4 km s^{-1}) away from the centroid proper motion of the cluster. While such stars are interesting for understanding cluster dynamics, they comprise a negligible fraction of the total population of a young cluster. The distribution of proper motions for these young clusters yield a 90% completeness

Table 1
Properties of Stellar Clusters

Name	R (deg)	R.A. (deg)	Decl. (deg)	PM(R.A.) (mas yr^{-1})	σ(PM R.A.)[a] (mas yr^{-1})	PM(Decl.) (mas yr^{-1})	σ(PM Decl.)[a] (mas yr^{-1})	d (pc)	σ(d)[b] (pc)
Serpens Main	0.5	277.51	1.08	3.08	0.57	−8.55	0.61	438	11
Serpens Northeast	0.8	279.54	0.37	2.61	0.41	−8.05	0.40	478	6
Serpens Far-South	0.7	277.91	−3.88	2.05	0.25	−8.96	0.28	383	2
LDN 673[c]	0.5	290.25	11.28	2.46	0.32	−10.25	0.24	407	16

Notes. The systematic error in parallax of 0.1 mas dominates the uncertainty in the distance.
[a] σ for proper motions are the standard deviation of the population.
[b] σ for distance is the standard deviation of the population, after correcting for uncertainties in parallax.
[c] Values calculated for all sources with parallaxes of S/N > 10.

Table 2
Populations of Stellar Clusters

Name	N_{20}[a]	N_5[a]	R_{stars} (deg)
Serpens Main	81	265	1.2
Serpens Northeast	80	251	1.5
Serpens Far-South	73	132	1.3
Distributed	105	519	…
Total Serpens Population[b]	339	1167	3.6

Notes.
[a] N_{20} and N_5: number of members with $\varpi/\sigma\varpi > 20$ and >5. Uncertainties ~5%; see text.
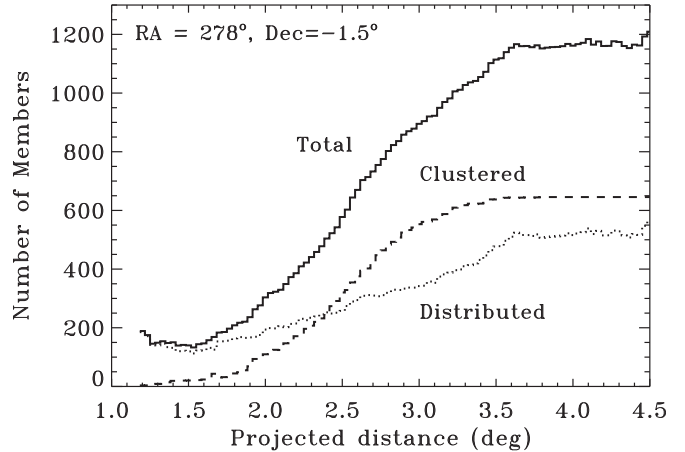[b] Includes the three subclusters and the distributed population.

Figure 5. The cumulative radial distribution of members from the approximate projected centroid of Serpens star formation at R.A. $\alpha = 278°$ and decl. $\delta = −1°.5$. The number of members is split into a total clustered population of stars in Serpens Main, Serpens Northeast, and Serpens Far-South, and a distributed population of stars that are not affiliated with those three optical clusters. The distributed population includes a few likely members of Serpens South and W40. Any epochs of vigorous star formation in the past ~30–50 Myr would have been identified either as a cluster or as a distributed population of stars. These memberships are statistical and therefore account naturally for interlopers. Some small numbers of stars are even more extended than shown here, including the LDN 673 and FG Aql groups.

within 4 km s^{-1}. Our analysis also preferentially excludes many stars with disks that are viewed edge-on. Variable young stars with associated nebulosity also have unreliable astrometry (e.g., V883 Ori, Lee et al. 2019; Sz 102, Fang et al. 2018) and would therefore tend to have high astrometric errors and/or proper motions and parallaxes that suggest nonmembership. Many binaries will also have been excluded from the *Gaia* DR2 astrometric catalog.

3.2. Searching for Isolated Groups of Stars

In the previous subsections, we identified subclusters and distributed populations of young stars in the Serpens Molecular Cloud. Past epochs of star formation may have produced populations that have since traveled away from the current epoch of star formation. The absence of these older populations places strong constraints on the star formation history, discussed in Section 5.4.

Some small groups of stars that are distant from the general boundaries of the active Serpens star-forming region may also be related to Serpens. A small overdensity of stars related to Serpens Northeast extends 2° (16 pc) northeast of the main cluster, while the Serpens Far-South overdensity extends ~3° to the southwest. A group of ~15 stars around LDN 673, including AS 353Aab, and a group of five stars around FG Aql have proper motions and distances consistent with Serpens membership, but are located ~100 pc away on the sky. These small groups are identified here only because of prior knowledge of their likely youth (Rice et al. 2006), and they would otherwise be challenging to detect. Other small groups of 5–20 young stars are likely to be present throughout the Serpens-Aquila field.

Expanding the proper motion cut to 5–10 mas yr^{-1} within the centroid of Serpens leads to the identification of IC 4665,

IC 4756, and NGC 6633 (e.g., Dias et al. 2002). The proper motions and ages of these clusters[14] together indicate that they are not directly associated with the clouds that are now forming stars in Serpens. Searching for clusters from 500 to 600 pc yields Collinder 359 (e.g., Lodieu et al. 2006; Cantat-Gaudin et al. 2018), a young cluster located at ~551 pc that may be related a previous epoch of star formation in Serpens.

No significant subclusters of young stars are identified in Serpens Cirrus, located at ~250 pc (see Section 4). Our blind search may have missed clusters at proper motions more than 5 mas yr^{-1} away from the centroid of the Serpens proper motion. However, the stars between 225 and 275 pc ($\varpi/\sigma(\varpi) > 20$) are distributed smoothly across the downloaded area. When divided into 0.5×0.5 deg^2 regions, the stellar distribution is nearly consistent with a Poisson distribution with 6.5 stars per 0.25 deg^2. The proper motion distribution also does not show any significant excess. A small number of young stars may be present and distributed across the region; however, no clusters are present with >15 young stars.

---

[14] The ages in Dias et al. (2002) should be accurate, because their pre-*Gaia* distances are within 5% of their *Gaia* DR2 distances.
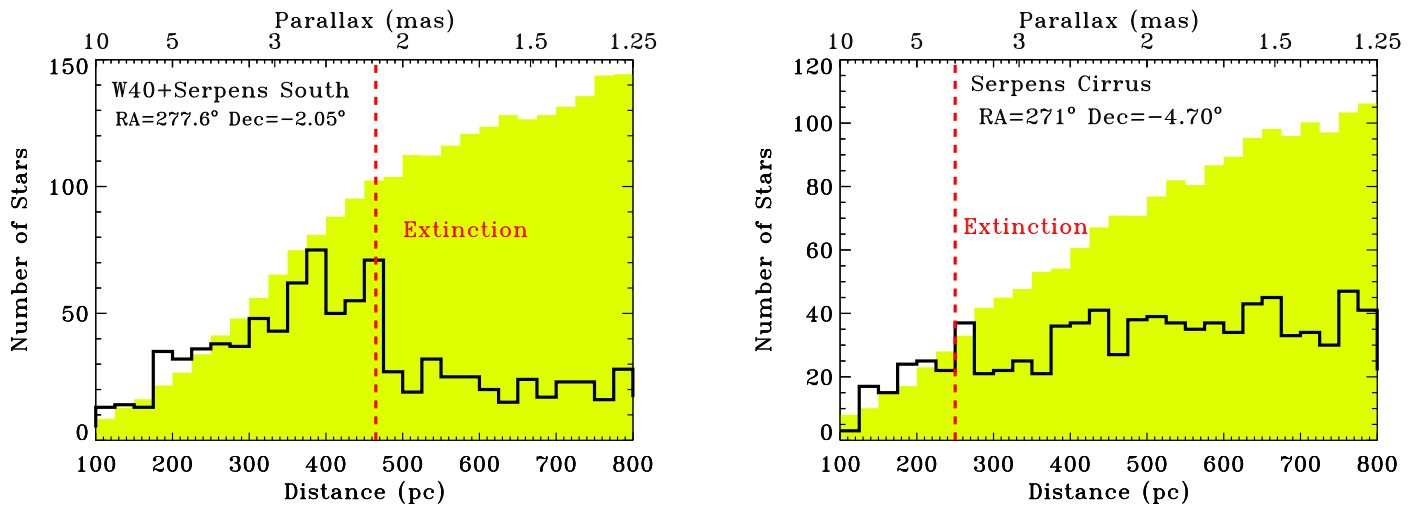
Figure 6. The number of stars vs. distance to (left) Serpens South and (right) Serpens Cirrus (black histograms), compared to off-cloud regions (yellow shaded histogram) that are scaled to the number of stars in Serpens South and Aquila between 50 and 250 pc, for stars with $\varpi/\sigma(\varpi) > 5$. The star counts vs. distance toward Serpens South drops sharply at ~460 pc because of the dark cloud; the apparent, though modest, discrepancy in star counts toward Serpens South at ~250 pc is artificial and well explained by synthesizing populations with a dark cloud at ~460 pc (see Figure 18 in Appendix B). The star counts in Serpens Cirrus fall off around 250 pc. Note that in Appendix B, the region of Serpens Cirrus is a different location, and Figure 18 shows results for stars with $\varpi/\sigma(\varpi) > 20$.

Our search for young stars does not include a rigorous evaluation of populations at >500 pc, including whether any young stars or star formation is associated with the Aquila Rift ($d = 600$–700 pc).

4. Measuring the Distance to Dust Extinction

In the previous section, we identified likely members of the Serpens-Aquila star-forming region, located at 350–500 pc and sharing a common proper motion. Dust extinction occurs over much wider areas than the stellar clusters. Clouds may be located at distances different from those of visually associated stellar clusters, and in any star formation region with a distance spread, the optical counterparts of a molecular cloud will be biased to members that are in the foreground of the cloud. In this section, we exploit the stellar distances of field stars to quantify the location and distance to dust extinction in the Serpens and Aquila clouds.

Figure 6 shows histograms of star counts versus distance for stars within a region, compared to those off-cloud from within 0°.5 in galactic latitude located south of the galactic plane. The star counts include stars with proper motions more than 3 mas yr^{-1} (6 km s^{-1} at 400 pc) from the centroid proper motion of Serpens members and with parallaxes with ϖ/σ $(\varpi) > 20$. The proper motion cut ensures that our selection focuses on field stars and is not influenced by any increase in young stars that are associated with the Serpens-Aquila complex. For stars within 0°.7 of Serpens South, the star counts drop dramatically at ~460 pc, indicating that the dust extinction occurs at approximately that distance. On the other hand, southwest of Serpens, the star counts deviate from the off-cloud region at ~250 pc.

This comparison establishes that clouds are present at multiple distances, and that measuring cloud distances with star counts is feasible. In this section, we first map the star counts with different distance cuts to determine the extent of the Aquila and Serpens clouds. We then quantify the distance to the dust extinction by simulating populations in different lines of sight.

4.1. Three-dimensional Maps of Dust

Figure 7 shows contours of the ratio of star counts with a range of distances, as a proxy for extinction at ~275 pc, ~450 pc, and ~650 pc. At each location in the map, the total number of stars[15] within some distance range is divided by the number of stars within some more nearby range of distance. For example, the dark clouds in Serpens can be seen in the ratio of the number of stars between 500 and 600 pc, $N(500$–$600)$, divided by the number of stars between 300 and 400 pc, N $(300$–$400)$. All ratios are normalized by the median ratio from regions in our map that are assumed to be free of extinction.

The contours of the star-count ratios show the locations where extinction occurs between those two distances.[16] The prominent extinction features associated with the Serpens star-forming complexes are located at 400–500 pc. Most of the extinction to the northeast of the Serpens star-forming cluster and in some adjacent dark clouds occurs at ~650 pc, called the Aquila Rift. Star counts at distances beyond >1000 pc demonstrate that the Aquila Rift extends across our entire field of view. The region to the southwest of the Serpens star-forming regions, here called Serpens Cirrus, has a deficit of stars between 300 and 400 pc, relative to the number between 30 and 250 pc. The color–magnitude diagram of stars toward Serpens Cirrus (Figure 8) confirms the ~250 pc distance to this dusty region, with a stellar locus that is offset by ~1 mag in A_V from the downloaded area (see Appendix A for the calculation of extinction vectors). The stars in front of the Serpens star-forming regions are not reddened relative to off-cloud regions, indicating the absence of any significant foreground extinction.

These comparisons provide an accurate assessment for the distance to the closest location where extinction occurs along the line of sight, if the extinction is sufficiently opaque. Extinctions of $A_G < 0.5$ may not be readily detectable in such star-count ratios for nearby regions, but significantly alter the

---

[15] $\varpi/\sigma(\varpi) > 20$ and proper motion >3 mas yr^{-1} from the Serpens centroid.
[16] The location of these dust features are robust to different choices for the expected ratio of number of stars in each distance bin, including corrections for galactic latitude.
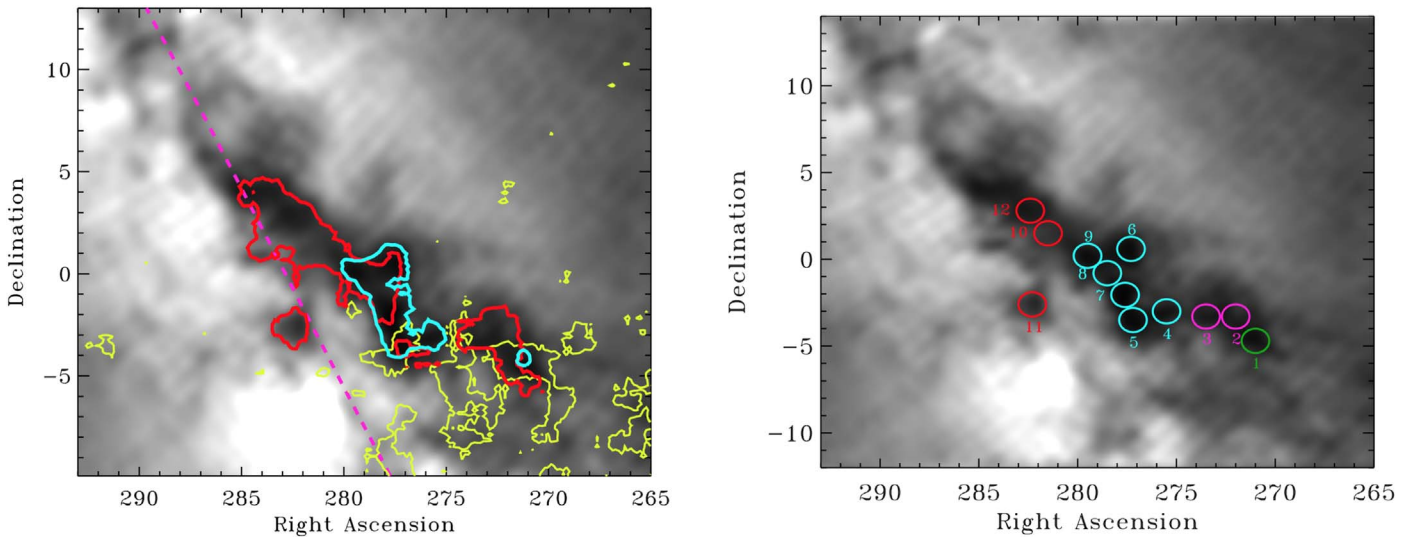
Figure 7. Left: contours of the star-count ratios, $N(d_2-d_3))/N(d_0-d_1))$, as a proxy for extinction at different distances. All values are corrected for the expected value at each galactic latitude. The yellow contour shows $N(300–400\ \text{pc})/N(30–250\ \text{pc}) = 0.7$ for extinction at ~250 pc, by comparing the number of stars between 300 and 400 pc to those between 30 and 250 pc. The blue and red contours show $N(500–600\ \text{pc})/N(300–400\ \text{pc}) = 0.4$ and $N(700–800\ \text{pc})/N(500–600\ \text{pc}) = 0.4$, both more optically thick than the yellow contours. The contours are created with $0°2 \times 0°2$ bins and smoothed with a two-dimensional Gaussian profile with an FWHM of nine bins. Right: the location of clouds with distances measured and listed in Table 3, color-coded by green ($d < 300$ pc), cyan (350–480 pc), pink (480–550 pc), and red (>550 pc).
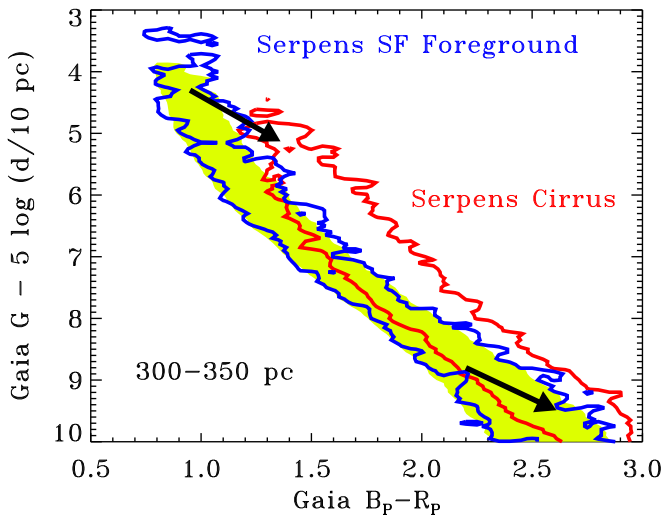

Figure 8. The color–magnitude diagram of all stars from 300 to 350 pc with $\varpi/\delta(\varpi) > 20$ and $G < 19$, for Serpens Cirrus (red contour, sources within a large rectangle from $\alpha = 262$ to 278 and $\delta = -12°$ to $-2°$), the foreground of Serpens (blue contour), and the rest of the field. Compared to the rest of the map, the stars in Serpens Cirrus are redder and fainter, seen in the different locations of the top of the main sequence, as expected for a population behind a cloud of dust. Extinction vectors (arrows) are shown for $A_V = 1$ (see Appendix A).

detected distribution of apparent magnitudes. Such star-count maps may therefore create the misperception that an optically thin, nearby cloud is actually located at a much larger distance.

4.2. Quantifying the Distance to Individual Clouds

The star-count maps described above reveal regions with significant extinction. To quantify the distance to regions of extinction, we compare the measured star counts versus distance to simulated star counts from off-cloud regions, after introducing a cloud at a given distance. Because the astrometric accuracy depends on brightness, the populations need to be simulated to quantify the distance and distance uncertainty to the extinction region. Appendix B describes our simulations of star counts versus distance for a sheet of extinction at some distance.

Table 3 and Figure 18 present our distance measurements to dust extinction for 12 circular areas on the sky. The dark clouds associated with young star clusters all have distances that are consistent with the measured distances to the young clusters (see Section 3). Along the Aquila Rift, the optically thick clouds are located ~500 pc to the southwest and ~600 to the northeast of Serpens. Serpens Cirrus is located closer to us than the Serpens star-forming clouds, as suggested in Section 4.1. The star counts to Serpens South and Serpens Main appear to have a deficit at ~250 pc, which is explained well by simulating *Gaia* data from off-cloud populations for a single, optically thick cloud at ~450 pc and should not be interpreted as indicating the presence of foreground dust at the distance of Serpens Cirrus (see also Figure 8). Stars that are in the foreground of the cloud may have a measured parallax (after accounting for uncertainties in parallax) that leads to a distance behind the cloud. Most stars that are physically behind the cloud are too faint to be detected by *Gaia*, and therefore no corresponding population of background stars has measured parallaxes that would place them in front of the cloud.

These distances are calculated by estimating the probability that the star counts for each region are from the same sample as the extinction-corrected off-cloud population. The probability is evaluated with a Kolmogorov–Smirnov test, for simulations with distance d and extinction A_G in a grid with a spacing of 5 pc and 0.1 mag. The star counts used for the Kolmogorov–Smirnov test have parallaxes with distances from 100 to 800 pc, measured with $\varpi/\sigma(\varpi) > 20$. The adopted distance in Table 3 corresponds to the grid point with the highest probability in the Kolmogorov–Smirnov test. The contours in Figure 18 show the parameter space that can be ruled out at 68% and 95% confidence. The d_{min} and d_{max} are then evaluated as the minimum and maximum distances that cannot be ruled out at the 95% confidence level. These 12 regions are selected

Table 3
Distances to Extinction Regions[a]

Number	Name	R.A.	Decl.	d (pc)	d_{min}[b] (pc)	d_{max}[b] (pc)	A_G[c]
1	Serpens Cirrus	271.00	−4.70	235	200	405	3.4
2	LDN 486[d]	272.00	−3.30	515	430	575	2.7
3	LDN 500[d]	273.50	−3.30	495	200	585	2.6
4	LDN 505[d]	275.50	−3.00	445	365	480	3.3
5	Serpens Far-South	277.20	−3.50	370	350	400	3.7
6	Serpens Main	277.30	0.60	445	385	475	3.4
7	Serpens South/W40	277.60	−2.05	460	425	495	4.4
8	Serpens	278.50	−0.80	415	375	470	3.0
9	Serpens NE	279.50	0.20	465	435	495	4.0
10	LDN 603[d]	281.50	1.50	585	480	590	2.0
11	LDN 566	282.30	−2.60	590	540	695	2.0
12	LDN 610	282.40	2.80	630	540	695	2.7

Notes.
[a] Calculated for projected circles with radii of 0°7 from the listed center.
[b] d_{min} and d_{max} are the minimum and maximum distances that cannot be ruled out at 95% confidence; see Figure 18.
[c] Extinction values are an average over the full region and are not reliable.
[d] LDN association is approximate.

in part because their best-fit extinction is $A_G > 2$ mag, which generates tighter constraints on the distance than if the extinction were lower; a few areas within our downloaded data set have high extinction but were also excluded.

The parent population for these measurements is obtained from regions that are thought to be unaffected by extinction and are located at a similar galactic latitude (within 0°5 of the centroid), but south of the galactic plane. Most extinction in the downloaded Serpens-Aquila area occurs at the north galactic latitude. In simulations with off-cloud populations located in the north of the galactic plane or separately in annuli around each region, the distances are similar but the extinctions are smaller.

The distance to a dark cloud corresponds to the front of that cloud, where the stellar density initially drops. Most dust structures in our image extend ∼1° (∼7 pc) in diameter on the sky and are therefore not deep along our line of sight. The assumption that these dust clouds are located at a single distance is reasonable, unless the structures are one-dimensional filaments aligned along our line of sight. However, each region may include multiple clouds located at different distances, and the clouds themselves are likely filamentary.

5. Discussion and Speculation

The *Gaia* DR2 view of the Serpens star-forming regions and the Aquila Rift reveals a complex set of star clusters and molecular clouds. The young stars are distributed across five different subclusters, three of which are detected by *Gaia* DR2 and have measured distances of 383–478 pc. The subclusters that are farthest apart, Serpens Far-South and Serpens Northeast, are separated by 35 pc in projected space but by 95 pc along our line of sight. These clusters are likely part of the same cloud complex, because the molecular gas is located at similar velocities (Dame & Thaddeus 1985; Davis et al. 1999; Dame et al. 2001). The Serpens star-forming cloud complex is therefore elongated along our line of sight and may be a branch of the much larger set of molecular clouds in the Aquila Rift, which has a distance of 600–700 pc to the northeast of the Serpens star-forming regions and ∼500 pc to the southwest of the active star formation.

Some light extinction also occurs to the southwest of the main Serpens complexes at ∼250 pc, called Serpens Cirrus. The distance to Serpens Cirrus confirms the accuracy of distance measurements to dust extinction from the maps of Straižys et al. (2003). However, this distance should not be applied to any known clusters of young stars, consistent with the conclusions of Prato et al. (2008). Serpens Cirrus is not entirely devoid of ongoing star formation; the dark cloud L483 hosts a protostar (e.g., Tafalla et al. 2000) and, with an approximate distance of 250 pc, seems to be associated with Serpens Cirrus. Some candidates identified by Dunham et al. (2015) in the southwesternmost region of their map, around (271, −4.5), may also be young stars. The separation in distance between the main Serpens star-forming clouds and the Serpens Cirrus is also consistent with the 3D extinction maps of Lallement et al. (2014).

The distances listed here are calculated from parallax measurements that have systematic uncertainties of ∼0.1 mas (Luri et al. 2018). The accuracy of VLBI measurements therefore exceeds that of *Gaia* DR2. The distance to two sources in Serpens Main[17] of 436 ± 7 pc, as obtained from VLBI measurements of maser emission (Ortiz-León et al. 2017), is consistent with our distance of 438 ± 11 (statistical 1σ error) ± 19 pc (systematic) to cluster members and 445^{+30}_{-60} pc (error bar corresponds to 95% confidence interval) to the cloud extinction. The VLBI distance to four sources in W40 and Serpens South of 436 ± 7 pc is also consistent with the distance of 460 ± 35 pc to the dust extinction to W40 and Serpens South. The number and color–magnitude diagram of stars in this region at ∼300–400 pc indicates a lack of optically thick dust within those distances, thereby excluding the possibility that Serpens South is located in the foreground.

Only five stars have astrometry from both *Gaia* and VLBI, and three of those stars have high astrometric noise, so we cannot evaluate systematic differences. The average proper motion of Serpens Main calculated here is consistent with the

---

[17] The VLBI distance to Serpens Main excludes the star GFM 65, which has a distance and proper motion that are highly discrepant from those of the Serpens Main cluster, indicating either that the observational uncertainties are underestimated for this source, that it is a remarkable runaway, or that it is a nonmember. The distance would place the star in front of the cloud.

VLBI proper motions of GFM 11 and EC 95. Of the four VLBI astrometric measurements in W40 and Serpens South, three have proper motions that are offset by a few mas yr^{-1} from the motion of the other Serpens clusters, consistent with a possible offset of $\sim$5 km s^{-1} in the proper motion of faint candidate members (see Section 5.3.2).

The distances to the Serpens star-forming clouds are consistent with the distances estimated by Green et al. (2015) from 3D dust maps obtained with Pan-STARRS (see also Green et al. 2018). However, the stilism (Capitanio et al. 2017) map of extinction suggests that the Serpens clouds are located at $\sim$700 pc, perhaps because of cloud confusion. Our distances are also remarkably consistent with the supposedly crude $\sim$440 pc photometric distance to HD 170634, located in Serpens Main, by Racine (1968) and Strom et al. (1974).

5.1. Evaluating Selected Past Membership Surveys

Gaia astrometry allows us to evaluate the optically bright candidate members of Serpens that have been identified by past surveys. Table 4 lists the number of objects in selected papers with a *Gaia* match,[18] with statistics following the classification of each match as either a robust nonmember or as consistent with kinematic membership. The contamination rates described here are generally measured to stars that are not located deep within the clouds. In regions with high densities of members, the contamination rates are likely much lower. On the other hand, in regions with low densities of members but with dark clouds, the contamination rates are likely underestimated because background objects will be too faint for detection by *Gaia*.

Nonmembership is assessed if the proper motion is more than 2 mas yr^{-1} (4σ) away from the Serpens centroid (Figure 9) or if the distance is 2σ away from the 370 to 490 pc range. Stars that have kinematics consistent with membership have proper motions within those ranges. Consistency with the Serpens distance is ignored if the parallax uncertainty is larger than σ $(\varpi) = 0.3$ mas, although inconsistency may be assessed for any parallax uncertainty. *Gaia* stars are considered a match if they are within 3″ of a *Spitzer* mid-IR position and 1″ of a near-IR or X-ray position. Most stars that are listed in catalogs but not matched with *Gaia* targets are optically faint, likely because they are located within or behind molecular clouds, because they are embedded in a dense envelope, or both.

The evaluation of memberships described here is based primarily on the census of Serpens from *Spitzer* maps of Dunham et al. (2015), which cover a wide area on the sky.[19] Because the Dunham et al. (2015) catalog establishes membership for most of the Gould Belt, this evaluation helps inform us of the reliability of different aspects of that catalog (Figure 10). Serpens Main and Serpens South have additional membership catalogs that are also evaluated here. For regions with optically thick dust, the *Gaia* matches are optically bright and are therefore more likely to be foreground nonmembers than either members or background contaminants, thus contamination rates for the youngest regions are unreliable. *Gaia* kinematics

---

[18] Including all *Gaia* DR2 targets with astrometry, with no limit on G_P but restricted to targets with excess astrometric noise <2 mas.
[19] Dunham et al. (2015) splits the population into Serpens, which includes Serpens Main and Serpens Northeast, and Aquila, which includes Serpens South, Serpens Far-South, and regions along the Aquila Rift to the southeast of Serpens. We divide these regions visually into additional subregions; see Table 4.
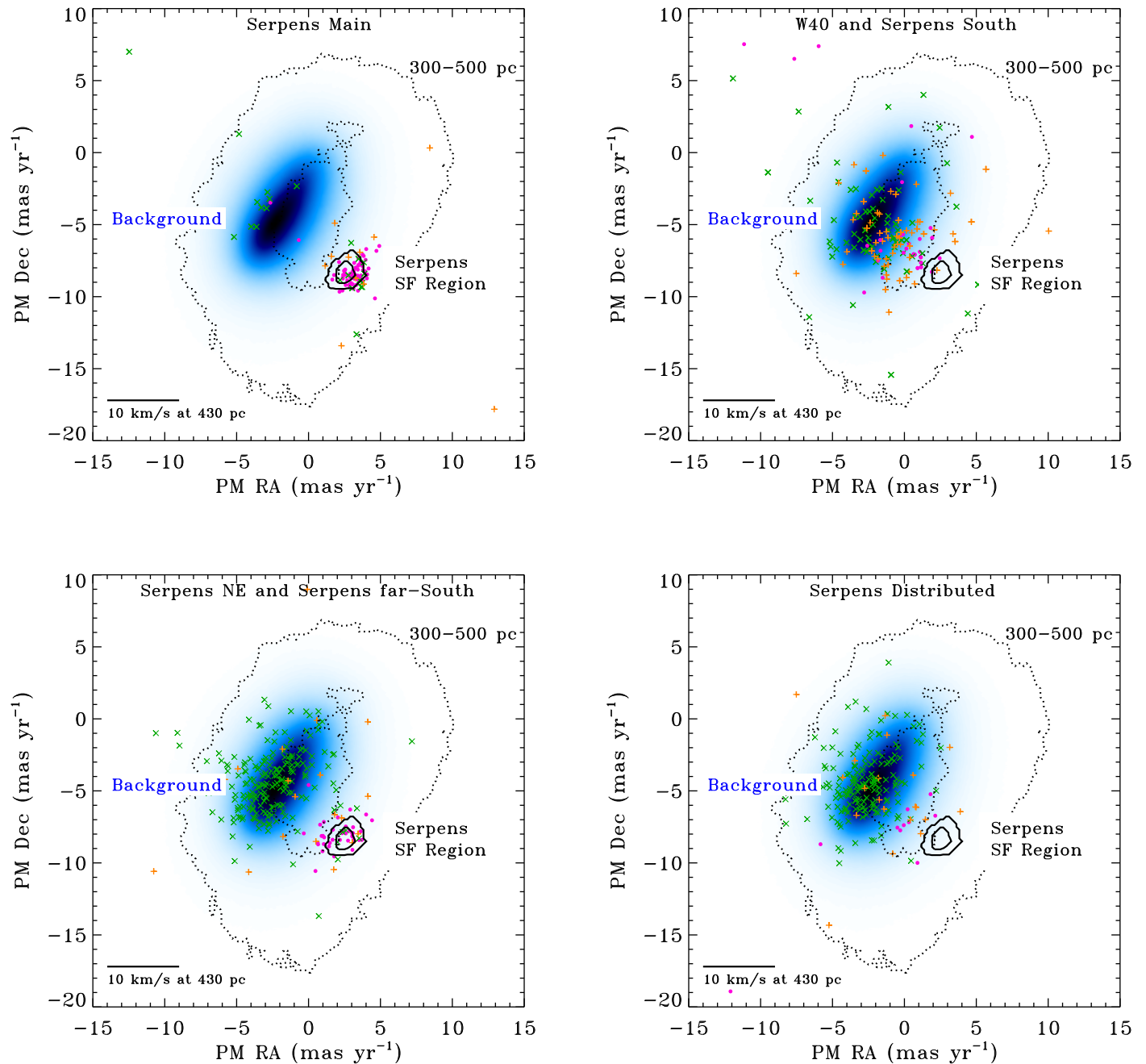
are also unable to probe the protostellar population, though the contamination rate of that population is likely to be low; Heiderman & Evans (2015) confirmed that 90% of protostar candidates in the Dunham et al. (2015) catalog have envelopes.

Most previously known stars with *Gaia* kinematics consistent with membership are located in Serpens Main. The *Gaia*-matched Class II objects from Dunham et al. (2015) have a membership probability of 86%, while the evolved (Class III) objects have a 50% probability of membership. Other IR and X-ray surveys have similar contamination rates. The 47% contamination rate for 74 *Gaia*-matched objects in the Eiroa et al. (2008) catalog is higher than expected. Inspection of these contaminants indicate that many were classified as candidates from near-IR photometry and lack spectroscopic confirmation.

For Serpens South and W40, very few sources that have been previously identified as candidate members can be evaluated with *Gaia*. The rejection rates from samples of disks and X-ray emitters (Kuhn et al. 2010; Dunham et al. 2015; Getman et al. 2017; Winston et al. 2018) with *Gaia* matches are 60%, while the rejection rate for Povich et al. (2013) is 80%. However, many of the objects in this region are clustered in proper motion and are offset by 5 km s^{-1} from the proper motion centroid of the three main optical clusters. These objects may be young, if the proper motion of Serpens South and W40 is offset from the rest of the Serpens complex (see further discussion in Section 5.3.2).

In most locations beyond the dense clusters, the *Gaia* matches to the Dunham et al. (2015) catalog demonstrate that the candidates are nonmembers, most with kinematics consistent with the background population. The classification of stars as background AGB stars by Dunham et al. (2015) are almost all confirmed. Most evolved stars outside of Serpens Main and Serpens South are also classified here as background objects; this category was intended to include diskless (class III) young stars with an expected contamination rate of 25%–90%. The protostars in Serpens Northeast and Serpens Far-South are likely robust. The one protostar and other matches to the southwest of the main Serpens clusters may be coincidental.

These contamination rates in the *Spitzer*-based population of Serpens and the Aquila Rift are likely not significant for some other regions evaluated by Dunham et al. (2015). The background population of AGB stars is much higher for Serpens, seen against the galactic plane, than for other nearby regions in the Gould Belt, which have higher galactic latitude. However, the *Spitzer*-based census of the Lupus V and VI star-forming region suffers from similar contamination of background stars, when evaluated with *Gaia* DR2 astrometry (Manara et al. 2018). The contamination in these populations will affect ratios of pre-main-sequence stars in different stages of evolution.

5.2. K-band Excess Disk Fractions of the Gaia Members

For young pre-main-sequence stellar populations, disk fractions may be used as a proxy for relative stellar ages (e.g., Haisch et al. 2001; Hernández et al. 2008; Mamajek 2009; Fang et al. 2013; Richert et al. 2018). In this analysis, we use 2MASS JHK_s photometry (Cutri et al. 2003) to directly compare the inner disk fraction of the *Gaia*-selected kinematic members of Serpens to the disk fraction analysis of W40 by Kuhn et al. (2010). Excess emission in the K_s band is used here as a proxy for emission from hot inner disks (see, e.g., Meyer et al. 1997). Although less sensitive than a mid-IR survey, 2MASS photometry covers the full region (unlike *Spitzer*), has

Figure 9. The proper motions of candidate young stars identified by Dunham et al. (2015) in the Serpens Main (top left), W40 and Serpens South (top right), Serpens Northeast and Serpens Far-South (combined into one plot, bottom left), and elsewhere in Serpens outside of these regions (bottom right), compared with the proper motions of the young stars in Serpens star-forming regions (solid contours at 0.2 and 0.5 times the peak value), all stars in our region with distances of 300–500 pc (dotted contours), and all background objects with distances >1000 pc (shaded blue contours), and objects with parallax errors that lead to uncertain membership (orange pluses). The candidate young stars that have *Gaia* DR2 distances consistent with the Serpens star-forming complex (purple circles) are clustered around the Serpens star-forming region, confirming membership, while objects with other distances (green x's) have proper motions that correspond to background stars. Many stars in Serpens South and W40 are clustered in proper motion a few mas yr^{-1} away from the main Serpens SF regions, which may be interpreted either as consistent with the field population at 300–500 pc or as a subcluster with a large scatter in proper motion.

fewer problems with blending and saturation in W40, and may be directly compared to a previous analysis of W40 using the same methodology.

Figure 11 shows kinematically selected sources from this work and X-ray-selected sources from Kuhn et al. (2010) on an $H − K_s$ versus $J − H$ color–color diagram. Following Kuhn et al. (2010), the 1 Myr Siess et al. (2000) isochrone is drawn and a reddening vector from $0.2\,M_\odot$ is used as an approximate separation between sources with and without K_s-band excess.

The majority of the stars within W40 are more deeply embedded than the population seen by *Gaia*. In W40, the K_s-excess fraction of ∼50% (after correcting for selection effects), while for the *Gaia*-selected sample, the K_s-excess fraction is <4%. The *Gaia* sources that do lie to the right also tend to be subject to higher extinction than the majority of the *Gaia* sources.

The lower inner disk fraction for the *Gaia* kinematic sample is consistent with the expectation that the optically bright

Table 4
Evaluating Past Membership Surveys

Catalog	Total	Matches	Nonmember PM > 4σ[i]	Nonmember ϖ > 2σ PM < 4σ[i],	Likely Member no ϖ PM < 4σ[i]	Likely Member ϖ < 2σ PM < 4σ[i]
Serpens Main						
Total Serpens Main	494	180	65	7	24	84
Dunham Total[ii]	227	104	20	5	16	63
Class 0/I, Flat	52	3	1	0	0	2
Disks	131	73	6	4	15	48
Evolved	39	28	13	1	1	13
(Likely AGB)	5	5	5	0	0	0
Giardino et al. (2007)	56	23	2	0	6	15
Eiroa et al. (2008)	253	74	33	2	14	25
Winston et al. (2010)	66	47	12	0	11	24
Gorlova et al. (2010)	19	3	0	0	1	2
Erickson et al. (2015)	63	54	17	1	1	35
Getman et al. (2017)	159	40	10	1	7	22
Serpens South and W40[iii]						
Dunham Total[ii]	725	153	126	5	18	4
Protostars	117	2	2	0	0	0
Disks	257	45	25	2	16	2
Evolved	351	106	99	3	2	2
(Likely AGB)	69	37	35	1	1	0
Getman et al. (2017)	645	18	12	0	4	2
Winston et al. (2018)	66	16	10	0	3	3
Povich Disks+Protostars	751	31	23	2	0	6
Protostars	281	5	2	2	0	1
Disks	470	26	21	0	0	5
Uncertain	244	8	6	0	0	2
Serpens Northeast[iii]						
Dunham Total[ii]	224	97	77	9	6	5
Protostars	16	3	2	1	0	0
Disks	36	14	3	5	3	3
Evolved	172	80	72	3	3	2
(Likely AGB)	41	32	32	0	0	0
Serpens Far-South[iii]						
Dunham Total[ii]	265	112	99	1	5	7
Class 0/I, Flat	10	0	0	0	0	0
Disks	34	14	6	0	3	5
Evolved	221	98	93	11	2	2
(Likely AGB)	45	40	39	0	0	1
Spatially Distributed Serpens[iii]						
Dunham Total[ii]	105	59	58	1	0	0
Class 0/I, Flat	4	1	1	0	0	0
Disks	3	2	1	1	0	0
Evolved	97	56	56	0	0	0
(Likely AGB)	55	52	52	0	0	0

Notes.
[i] Here, 4σ in proper motion is ∼2 mas yr^{-1}. The distance criterion of 2σ is based on parallax uncertainty.
[ii] Likely AGB stars are excluded from all totaled numbers.
[iii] Stars labeled "Aquila" by Dunham et al. (2015) are allocated to different regions as follows—Serpens Northeast: decl. > −1°, Serpens South+W40: decl. > −1°; Serpens Far-South: within 1.5° of (277.9, −3.9); Serpens Distributed is everything else labeled "Aquila."

populations are older stars, while the younger stars and protostars are located deep within the molecular cloud. This radial age gradient is often seen in star-forming regions (Getman et al. 2014, 2018; Jose et al. 2016), either because older stars drift outward or because the molecular material rapidly disperses after forming stars (see Section 5.3.3). This
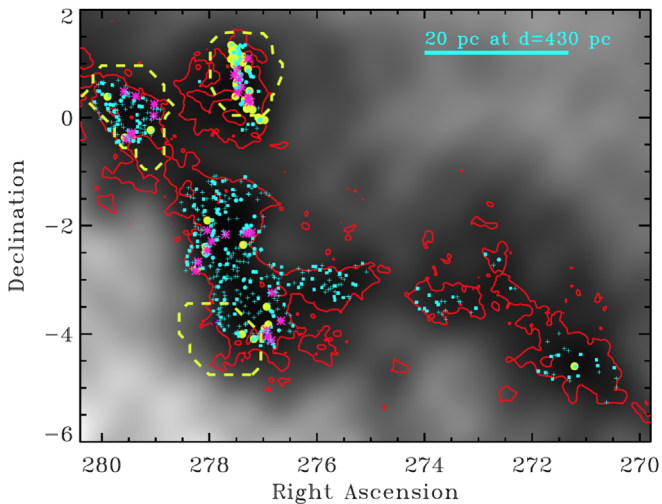
Figure 10. Objects from the Dunham et al. (2015) *Spitzer* catalog of candidate members of the Serpens-Aquila star-forming complexes, plotted against the star-count map from Figure 1. The yellow circles (disks and protostars, as classified by Dunham et al. 2015), purple asterisks (diskless members), and yellow squares (AGB stars) have distances and proper motions consistent with membership, with proper motions within 4 mas yr^{-1} of the Serpens centroid and distances within 2σ of 380–480 pc. Most of the evolved (diskless, shown as small pluses) candidates and the candidates identified as background AGB stars (small squares) by Dunham et al. (2015) are background AGB stars. The blue objects (with classifications the same shape as above, though smaller) are likely nonmembers. The objects identified as disks and protostars (red circles) are almost all located in one of the major Serpens clouds. The confirmed members are tightly confined to four specific regions of star formation; virtually no candidates from Dunham et al. (2015) are identified as members in the extended regions of what was then termed the Aquila Rift. The *Spitzer* observations focused on regions with $A_V > 5$ (red contours), as measured by Cambrésy (1999). The three optical clusters identified in this paper are shown in yellow contours.

comparison of near-IR disk fractions are also influenced by selection effects, because local extinction from circumstellar disks may hamper the sensitivity of *Gaia*, and by differences in applying this technique to samples with very different extinctions and mass distributions (see also Soderblom et al. 2014 for a description of the uncertainties in using disk fractions for age estimates). An evaluation of disk presence with mid-IR photometry would yield higher disk fractions. Nevertheless, the 4% fraction of stars with inner disks is much lower than would be expected for a very young region, such as W40, and may indicate that the optically bright population has an average age of 5–10 Myr. The more embedded regions that were not detected by *Gaia* have much younger ages.

5.3. Describing the Clusters

The young stars in Serpens are preferentially located in a few clusters. Figure 12 shows color–magnitude diagrams for the three optical clusters and for the distributed population of young stars in the region. The magnitudes are corrected for the average distance to each cloud but are not corrected for extinction. Individual stellar distances are used for the distributed population.

Almost all candidate members are located above the main sequence and are consistent with the pre-main-sequence locus, despite a selection that did not include photometry. These candidates therefore have a very high membership probability, even without spectroscopic confirmation. Table 7 in Appendix C provides the *Gaia* DR2 astrometry and photometry for these high-

probability objects. A complete (rather than a statistical) sample of members would require spectroscopic confirmation of stars with low-to-modest probability of membership.

The stellar positions of likely members are compared to the unreddened PARSEC isochrones (Bressan et al. 2012; Marigo et al. 2017) using the BT-Settl colors (Allard 2014). If we infer a typical extinction of $A_V \sim 2$ mag (ignoring differential reddening within a cluster and the effects of accretion), then this *Gaia* DR2 identification of members is sensitive to $\sim$0.2–0.3 $M_\odot$, with a completeness that is high in low-extinction regions and for higher masses. The estimated cluster ages for this extinction range from <1 Myr for Serpens Main to $\sim$3 Myr for Serpens Far-South and the distributed Serpens population. These ages are younger than expected for the (K-band excess) disk fraction of 4%. Resolving this tension will require analyses of individual stars, which is beyond the scope of this paper, and the resolution of long-standing challenges with ages of young stars (see review by Soderblom et al. 2014). However, even if the oldest populations have ages of 10 Myr, the challenges described below are still robust, just scaled to an older age.

5.3.1. Serpens Main

Serpens Main was the first young subcluster in this region to be systematically evaluated (Eiroa & Casali 1992). The dust-extinction distance of 445^{+30}_{-60} pc is consistent with the stellar distance of 438 pc and the VLBI distance of 436 pc from Ortiz-León et al. (2017). The Hertzsprung–Russell (HR) diagram reveals a luminous population, indicating a young ($\sim$1 Myr) age, and a large dispersion in luminosity expected for such a young cluster (see discussion in Soderblom et al. 2014).

The cluster is rich in both protostars and disks, with the protostars concentrated in small regions within this cloud. If the *Gaia*-based contamination rate applies to the disks and diskless populations from Dunham et al. (2015), the protostar/disk fraction would be $\sim$0.42 and the disk/diskless fraction would be $\sim$5.8. This subcluster is evolved enough for many members to be optically bright. No gradient in proper motion is detected, so most of the visible stars have not traveled far from their birth location.

5.3.2. Serpens South and W40

W40 and Serpens South are the most populous regions in the Serpens region. However, the protostars in Serpens South are located deep within the molecular cloud, which is why it was not recognized as such an active region of star formation until mid-IR surveys (Gutermuth et al. 2008). Dunham et al. (2015) identified 374 IR-excess sources (protostars and disks), while Povich et al. (2013) and Mallick et al. (2013) identified 983 and 1202 likely members from 2MASS and IRAC analyses, respectively.[20] The total population of Serpens South and W40 may be similar to the total membership of other Serpens clusters, depending on the contamination rate.

The combined W40 and Serpens South region has a VLBI parallax distance of 436 pc (Ortiz-León et al. 2017). The optically thick extinction to this combined region occurs at

---

[20] The Mallick et al. (2013) sample is a superset of the Povich et al. (2013) sample. Dunham et al. (2015) required a detection in the MIPS 24 μm band, while Povich et al. (2013) and Mallick et al. (2013) required *Spitzer* detections only in IRAC 3.6 and 4.5 μm images. Many additional protostar candidates have been identified with *Herschel* (Bontemps et al. 2010; Könyves et al. 2015). All samples produce targets that are clustered along the filaments associated with Serpens South and W40.
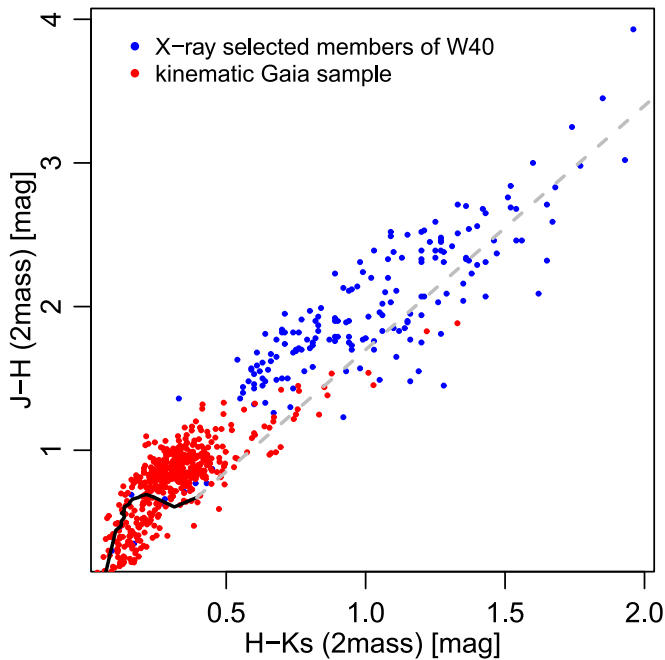
Figure 11. 2MASS color–color diagram for the kinematically selected sample (red) and X-ray-selected cluster members from W40 (blue, from Kuhn et al. 2013), with a 1 Myr isochrone from Siess et al. (2000). A larger fraction of W40 members than *Gaia* kinematically selected members have a *K*-band excess from an inner disk. The *Gaia*-selected sample is only the surface population of slightly older, optically bright stars within a large complex that harbors a rich population of protostars in several sites of ongoing star formation.

$\sim460 \pm 35$ pc. We therefore conclude that the W40 and Serpens South clusters are likely located at the same distance, as inferred by Ortiz-León et al. (2017), so that their VLBI parallax distance should be adopted for both Serpens South and W40 (see also an independent analysis of *Gaia* DR2 astrometry by Ortiz-León et al. 2018). Only a few candidate young stars in this area are detected by *Gaia* DR2, with typical distances of ~410 pc. These stars may be biased to a distributed population of young stars in the foreground of the dark cloud.

Objects in Povich et al. (2013) and Dunham et al. (2015) with spatial locations and parallaxes consistent with Serpens membership have proper motions that are offset from the Serpens centroid by ~2.5 mas, or 5 km s^{-1} (see Figure 9). Three of the four stars W40 and Serpens South with VLBI astrometry also have proper motions consistent with this offset in proper motion. In contrast, Figure 13 shows that a cluster of stars (brighter than $G < 19$) have proper motions consistent with the wider Serpens region. No other overdensity is detected at the visual location of Serpens South and W40 (for stars with the offset proper motion) or in proper motion (for stars located in W40 and Serpens South).

One interpretation is that Serpens South and W40 have projected velocities on the sky that are offset by 5 km s^{-1} from the other clusters within Serpens. Most of the candidate members from the Povich et al. (2013) and Dunham et al. (2015) catalogs are optically faint ($G > 19$) and are excluded from our broader overview. The candidate members with proper motions consistent with the larger Serpens complex would then be distributed members, located in the foreground of the dark cloud rather than within the active star-forming clouds. An alternate explanation is that the candidate members with offset proper motions in Figure 9 are field stars, because they overlap with the distribution of proper motions for stars from 300–500 pc over the full downloaded area.

The offset of ~5 km s^{-1} on the sky is larger than expected based on the similarity of line-of-sight velocities to cold gas in the W40 and Serpens South molecular clouds (Nakamura et al. 2011; Shimoikura et al. 2015), compared to the velocities of Serpens Main and Serpens Far-South (Dame & Thaddeus 1985; Davis et al. 1999). However, some expansion is seen in the gas in W40, which is related to the H II bubble (Zhu et al. 2006; Pirogov et al. 2013; Shimoikura et al. 2015), and may contribute to a larger dispersion in proper motions for newly formed stars. The proper motions of the faintest objects may also suffer from larger systematic errors than expected. Distinguishing between these explanations will require spectroscopy of candidate members to evaluate youth.

5.3.3. Serpens Northeast

The stellar population of Serpens Northeast is located at 478 pc, consistent with the dust-extinction distance of 460 ± 35 pc. This subcluster is the most distant cluster of young stars within the Serpens star-forming cloud complex, as defined in this paper. Much of the optically thick dust in the Aquila Rift is also located to the north and east of Serpens Main. This distance may indicate some connection between Serpens star-forming regions and the Aquila Rift, because the clouds in the Aquila Rift near Serpens Northeast are located at ~600 pc. Serpens Northeast includes some stars $\sim2°$ (16 pc) northeast of the main optical cluster, located along the direction of the Aquila Rift dust cloud.

The optical appearance of Serpens West is visually split into two by an optically thick dust cloud, like a dust sandwich with the optically bright stars around the dust. Some protostars and disks are present within the cloud (Dunham et al. 2015). The location of stars on the color–magnitude diagram, as well as the (candidate) protostar/disk ratio, suggests that Serpens Northeast is older than Serpens Main but younger than Serpens Far-South. The populations north and south of the cloud are indistinguishable in distance.

The projected morphology of Serpens Northeast, with an optically bright population around the dust, may be explained if the stars were either formed in a centralized factory and flung outward, or if the stars were born near their current location and have been eroding the nearby cloud. The stars in the northern half of the sandwich have proper motions of $+0.15$ mas yr^{-1} relative to the proper motions of southern stars (Table 5 and Figure 14). However, if both populations had formed at the same spatial location, they would have had to have been flung out ~20 Myr ago, older than the age estimated from the color–magnitude diagram. Even more challenging, the standard deviation in the proper motions is 0.4 mas yr^{-1}, so many of the stars in the north are traveling south, and vice versa, at a velocity consistent with the velocity dispersion measured for protostars (e.g., Kirk et al. 2010; Heiderman & Evans 2015). Populations to the east and west also do not correspond to a past origin in some centralized location within the present-day cloud.

Some of these stars have either come from the opposite direction of the current location of the dark cloud, or their proper motions have already been altered by internal dynamics within the small cluster. The optically bright stars have likely formed out of what is now an eroded cloud, while a few protostars are still forming where the cloud is still optically thick. This erosion does not conflict with the possibility that stars are also being flung out from the birth filament at the lower velocities that have been observed in the Orion Nebula (Mairs et al. 2016; Stutz & Gould 2016).
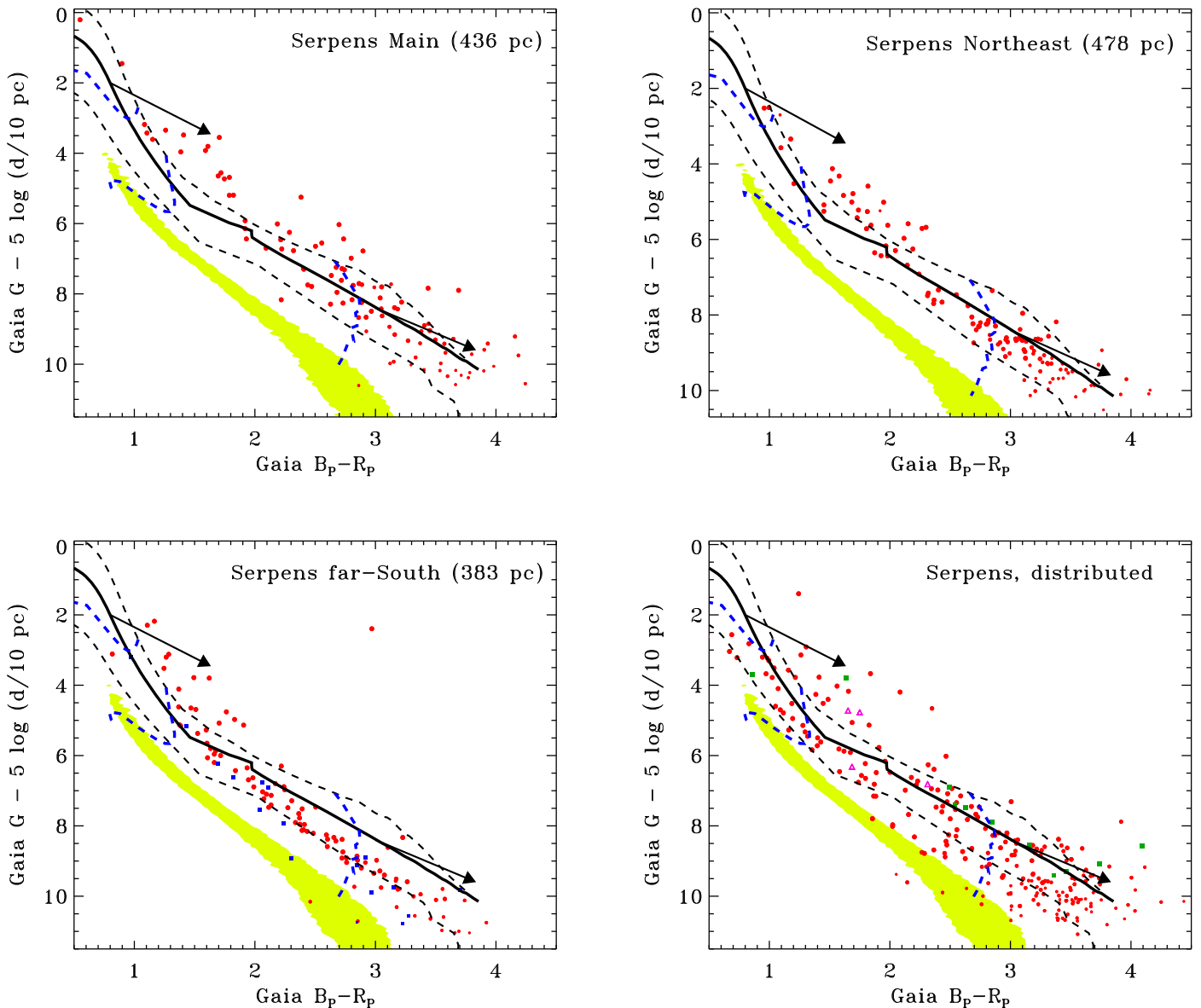
Figure 12. Color–magnitude diagrams of young clusters in Serpens, compared with unreddened isochrones of 1, 2.5, and 10 Myr and evolutionary tracks for stars with 2.0, 1.0, and 0.3 $M_\odot$ (Bressan et al. 2012; Marigo et al. 2017). The size of points indicates the accuracy of the parallax measurement, from $\varpi/\sigma(\varpi) > 20$ (largest) to $\varpi/\sigma(\varpi) = 5$ (smallest). The distance-corrected magnitudes are calculated assuming a single cluster distance, as listed. The lower left panel includes the small group at $\alpha = 276$, $\delta = -6$ (blue squares). The lower right panel includes all high-probability members that are not associated with any of the three main optical clusters, including the LDN 673 group (407 pc, green asterisks) and the FG Aql group (408 pc, green squares); individual stellar distances are used for the distributed population. The main sequence (yellow shaded region) is calculated from all stars in our field between 50–250 pc and with $\varpi/\sigma(\varpi) > 20$.

5.3.4. Serpens Far-South

This cluster pokes out of the extreme southern end of the dark cloud, directly south of the Serpens Main and Serpens South clusters. The optical cluster is located ∼1° southeast of the optically thick dust in Serpens Far-South, where some protostars are present (Rumble et al. 2015). This region is not well studied. The *Spitzer* observations of Serpens (e.g., Dunham et al. 2015) were defined by the dust maps and therefore missed the optical counterparts. Sh 2-62, powered by the Herbig Be star MWC 297, is located on the eastern end of the cluster. The H II region Sh 2-61, powered by the Herbig Be star HBC 284, is projected on the southwest edge of the cluster but has *Gaia* astrometry consistent with a background object. Many of the candidate young stars in the Dunham et al. (2015) catalog are found to be nonmembers. Based on the color–

magnitude diagrams, this region is the oldest of the active star-forming complexes in Serpens.

An overdensity of stars extends 2°.8 (19 pc) to the southwest of the main optical cluster, ending in a group of ∼15 stars located at $\alpha = 276°$, $\delta = -6°$ to $-7°$. The proper motion of this small group of PM(R.A.) = 1.7 mas yr^{-1} and PM(decl.) = -8.3 mas yr^{-1} is offset by 0.7 mas yr^{-1} from the main cluster, so this may be a distinct group from Serpens Far-South. The location of these stars on the color–magnitude diagram indicate a similar age to the Serpens Far-South cluster.

5.3.5. LDN 673

This dark cloud is located ∼120 pc from the main Serpens star-forming regions. The cloud has formed ∼15 members bright enough to be identified with *Gaia*, with a mean distance

Table 5
Proper Motions of Stars in Serpens Northeast[a]

N	R.A. Range	Decl. Range	PM(R.A.)	σ(PM–R.A.)	PM(Decl.)	σ(PM–R.A.)	d	$\sigma(d)$
21	279.2–279.6	−0.6 to −0.1	2.69	0.35	−8.18	0.40	472	15
30	279.2–279.6	0.2 to 0.8	2.51	0.38	−8.05	0.39	489	20
20	279.65–280.1	0.0 to 1.0	2.42	0.40	−8.21	0.31	484	19
12	278.8–279.2	0.0 to 1.0	2.93	0.38	−8.03	0.81	482	21

Note.
[a] For stars with $\varpi/\sigma(\varpi) > 10$, from 440 to 530 pc, and within 1.7 mas yr^{-1} of the proper motion centroid.
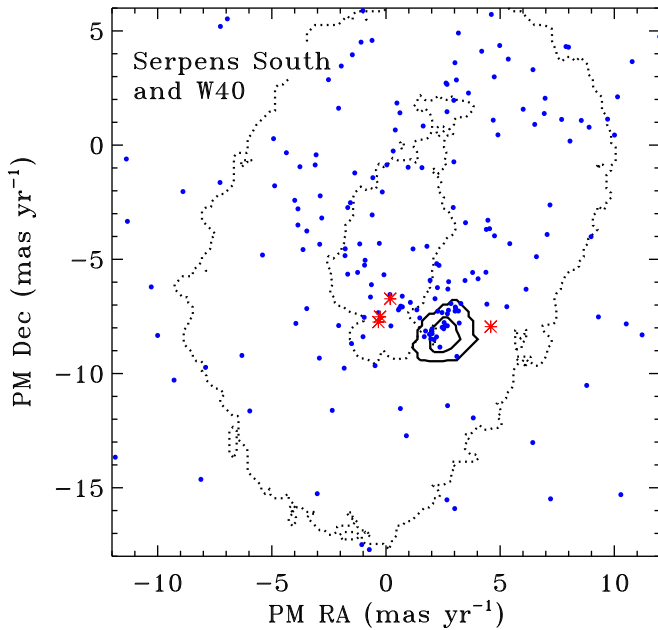
Figure 13. Proper motions for stars brighter than $G < 19$ located visually within Serpens South and with parallaxes indicating distances of 390–490 pc (blue circles), compared with four proper motions of stars in W40 and Serpens South as measured by VLBI (red asterisks).

Figure 14. Proper motions of stars in Serpens Northeast, showing current positions (circles) and positions 2 Myr ago (asterisks) for stars with $\varpi/\sigma(\varpi) > 20$. The colored squares have $10 < \varpi/\sigma(\varpi) < 20$ and are included in the analysis, but with past positions not shown for ease of visualization. Purple diamonds show protostars and disks from the Dunham et al. (2015) catalog. The blue and yellow colors show specific overdensities to the north and south of the cloud, with proper motions inconsistent with an origin within the present-day cloud. The green outer regions are consistent with this interpretation. Red circles shown here are likely members that are excluded because they are outside the current overdensities. The average proper motion of Serpens Northeast has been subtracted from all stellar proper motions shown here.

of 407 pc and a mean proper motion similar to that of Serpens (see also the identification of this group by Rice et al. 2006). The members of this subcluster, including AS 353A (with the associated HH object HH 32 discovered by Mundt et al. 1983) and V536 Aql, have similar colors and distance-corrected brightness to those in other Serpens regions.

5.3.6. FG Aql Group

We identify five stars, called here the FG Aql Group, with distances of ∼400 pc and proper motions consistent with Serpens. On the sky, this small group is located ∼60 pc southeast of the ongoing star formation. This small group of stars is identified here only because Prato et al. (2008) listed them as possible young stars, following past identification and incorporation into the Herbig & Bell (1988) catalog.[21] This group would have been detected with an analysis that combined a nearest neighbor criterion and photometry.

5.4. The Star Formation History of the Serpens Molecular Cloud

Within the Serpens cloud complex, about 60% of the optically bright stars are located within one of the three main (optical) clusters. These past bursts of star formation, and the ongoing burst in Serpens South, are concentrated in specific spatial locations. Some additional star formation has also occurred beyond this projected region, including in LDN 673 and the FG Aql Group.

The population found by the *Gaia* astrometric selection is likely older than the members that are located deep in the molecular cloud. An age gradient is present within the full Serpens star-forming region, with Serpens South as the youngest subcluster and Serpens Far-South as the oldest. An age gradient is also present within each subcluster. In the Serpens Northeast and Serpens Far-South subclusters, the protostellar population found by Dunham et al. (2015) and Rumble et al. (2015) is still located within the cloud, while the optical population is likely

---

[21] Candidate members HBC 684 and FG Aql/G3 have astrometry consistent with background objects and are likely nonmembers, as do several other candidate young stars in this region that are listed in the Herbig & Bell (1988) catalog.
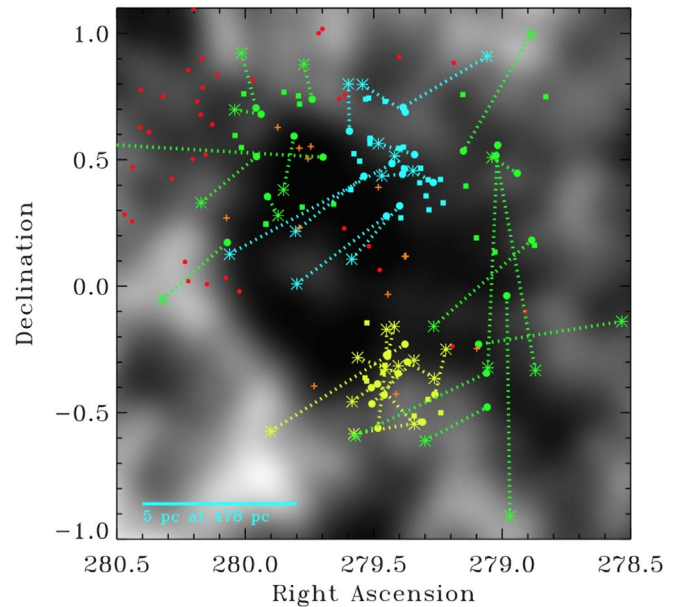
older. Such age gradients are widely observed on other star-forming regions (e.g., Mairs et al. 2016; Getman et al. 2018).

The age gradients may be caused by cluster dynamics or a by a change in the site of active star formation. In the hierarchical star formation scenario of Vázquez-Semadeni et al. (2018), an age gradient is expected, but is most apparent for ~20 Myr old stars, because given a scatter in initial velocities, the older stars have longer time to disperse. However, the standard deviation in proper motions of ~0.5 mas yr^{-1} (~1 km s^{-1}) within each subcluster is inconsistent with a dynamical explanation for an age gradient; neither are the optically bright stars the ones that happened to be flung out. Instead, feedback from these stars (e.g., Cunningham et al. 2018) has likely eroded away the nearby molecular material over several Myr.

A cluster located at 430 pc with a velocity dispersion of ~1 km s^{-1}, with no internal dynamics, would expand by ~1° every 10 Myr. Over ~50 Myr, any clustered star formation would likely remain in a cluster and would likely not move far from the birth site, unless the velocity dispersions were significantly larger than those observed here. Two older clusters, Collinder 359 and IC 4665, were found here with *Gaia* DR2 astrometry (see also Cantat-Gaudin et al. 2018) and may be related to a burst of star formation tens of Myr ago. Collinder 359, located at a distance of 551 pc, is visually separated by 85 pc on the sky from the northern clusters of Serpens. Given the relative proper motions (Cantat-Gaudin et al. 2018), the cluster would have overlapped with Serpens Northeast (in projected space) 16 Myr ago, which is likely younger than the cluster age, estimated to be ~60 Myr by Lodieu et al. (2006). IC 4665, located at 350 pc, is a less promising candidate. The cluster, located at a distance of 350 pc, has a proper motion that would have also placed it visually northeast of the Serpens clouds 13 Myr ago, much younger than the estimated age of 40 Myr by Dias et al. (2002). Any visual association between IC 4665 and Serpens is likely coincidental, while the relationship between Collinder 359 and Serpens is unclear.

The lack of clusters and young stars beyond this immediate region indicates that the star formation in Serpens is a recent burst. Because our selection of Serpens members is independent of any photometric criterion (other than sufficient brightness for accurate astrometry in *Gaia* DR2), we would have detected any significant star formation that occurred in the recent past. Even if the distributed young stars are entirely from a previous epoch, the star formation rate over the past 50 Myr must have been at least ~20 times lower than the current rate. Thus, it seems likely that the recent bursts of star formation are the first generation of stars in this cloud complex. The possibility that a small burst 30–60 Myr ago in Serpens could have created Collinder 359 would reinforce the fact that the star formation is very bursty.

The current epoch of star formation began within a few Myr of each other in regions that are separated by distances of 20–100 pc. The typical sound speed in a molecular cloud of ~0.2 km s^{-1} leads to a crossing time of 100–500 Myr (see, e.g., the discussion of Upper Sco in Preibisch & Zinnecker 1999; Slesnick et al. 2008); a shock would therefore need to travel at ~20–100 km s^{-1} to connect these distant regions on a Myr timescale. The large separations between these groups are some of the more difficult-to-explain aspects of star formation in this region. This situation is not unique to the Serpens-Aquila region, as many massive star-forming regions contain several discrete clusters of stars separated by tens of parsecs (Kuhn et al. 2014). A prominent example is the NGC 6357 star-forming region, which contains three Orion-like clusters separated by ~10–15 pc (Townsley et al. 2014). NGC 6357 itself is separated from the star-forming region NGC 6334 in the same giant molecular cloud complex by a projected distance of ~60 pc. On the other hand, the Orion Nebula Cluster and the broader Orion region have undergone several distinct epochs of star formation (e.g., Beccari et al. 2017; Kounkel et al. 2018). This puzzle for Serpens is exacerbated, or at least now better established, by the lack of young stars from previous epochs of star formation, as would be seen over a very large area on the sky.

Several mechanisms could potentially induce near-simultaneous star formation at different locations in molecular clouds. For example, gravitational instabilities in a long, filamentary cloud can produce regularly spaced regions of star formation activity (Gehman et al. 1996). Alternatively, the assembly of giant molecular clouds through a series of cloud–cloud collisions (e.g., Ibáñez-Mejía et al. 2017) could produce multiple sites of star formation. In both Serpens Main and W40/Serpens South, kinematic studies of clouds suggest a history of cloud–cloud collisions (Duarte-Cabral et al. 2010; Nakamura et al. 2017; Shimoikura et al. 2018). However, while cloud–cloud collisions may be the local trigger for a burst, it is hard to imagine that any sort of cloud–cloud collision could occur at specific sites spread over such large distances, without any star-forming collisions in the recent past elsewhere along the clouds.

In principle, compression from a shock wave from a supernova or winds from hot stars could have triggered star formation in all three regions of the molecular cloud. However, there are no indicators that a nearby supernova has occurred. The 40 Myr old cluster IC 4665 (Dias et al. 2002) and Collinder 359 may have had a sufficient number of hot stars for winds to sweep up some gas, thereby precipitating local cloud–cloud collisions across a wide region on a timescale consistent with requirements on the travel time for a shock, though this explanation seems overly ad hoc. In any case, given the large available gas reservoir in the Serpens-Aquila region (Zeilik & Lada 1978; André et al. 2010) and the extreme youth of the stellar population of the region, it is likely that the region is still in the early stages of its star formation history, the star formation rate is accelerating, and the observed stars are just the first to form.

6. Conclusions and Prospects for the Future

We have performed an initial evaluation of the Serpens star-forming complexes and the Aquila Rift using *Gaia* DR2 astrometry. The optically bright young stars are concentrated in three clusters in the Serpens star-forming region, with distances from 383 to 478 pc and relative velocities between the clusters of ~1 km s^{-1}. Some young stars are distributed throughout the region and may have formed in smaller groups. The distances to optically thick dust extinction of these regions are consistent with the distance to the stellar populations. While Serpens members are identified using only astrometry, the *Gaia* photometry establishes that a tight selection in proper motion and distance generates a robust sample of young stars. The populations identified here are older and more widely distributed than had been known previously, complementing past mid-IR surveys that had identified populations within the dark molecular clouds that are not detectable with *Gaia*.

Some dust is present in the Serpens Cirrus, located to the southwest of the Serpens star-forming regions, with a distance of ~250 pc, consistent with past distance measurements to dust extinction in this region by Straižys et al. (2003). The Serpens

Cirrus dust is not very opaque ($A_V \sim 1$ mag when averaged over a large region) and is not associated with significant star formation, although the protostar L483-mm and perhaps a few other young objects are forming in this area. The dust in the Aquila Rift is located $\sim$600 pc to the northeast and $\sim$500 pc to the southwest of Serpens. Because the distance of the Aquila Rift tends to increase smoothly from the southwest to the northeast, the Aquila Rift may be one huge complex that includes Serpens star-forming regions. While it might seem surprising for the cloud to extend 300 pc along our line of sight, the Aquila Rift spans at least 250 pc across our full field of view, when projected on the sky.

The active star formation in Serpens over the past few Myr has occurred across a distance of $\sim$100 pc, in distinct sites that are typically $\sim$5 pc across. The absence of an older population indicates that little star formation occurred prior to this current activity. This strongly suggests some sort of external trigger traveling at 20–100 km s^{-1} to generate the star formation. If the ages are older than inferred here, then the speed of the trigger could be reduced but would not alter the general picture.

In Serpens Northeast, several protostars are located within the optically thick cloud, while optically bright stars are located north and south of the cloud, like a dust sandwich. The proper motions of these optically bright stars indicate that they were likely formed near their present locations and have eroded way their parent molecular cloud. Their positions and proper motions are inconsistent with having been formed in a central star formation factory and then flung out to their current location.

This evaluation should be treated as an initial analysis of the *Gaia* view of the Serpens-Aquila region. Future data releases will improve astrometric precision for optically fainter sources, which will allow us to increase sample sizes and thereby better probe the low-mass and embedded populations. The analysis of line-of-sight dust extinction should improve by adding multiple regions of dust and by incorporating the brightness and colors of objects, rather than just star counts. A full census of the population should assign membership probabilities to each star. Analyses of individual stars would improve age and mass estimates.

Despite these caveats to our work, we are still able to identify a new, optically bright population in Serpens that was not previously known, as well as resolve nagging doubts about the distances to W40/Serpens South and other regions in the Aquila Rift and Serpens Cirrus. This work was performed almost exclusively with *Gaia* data.

Appendix A
Extinction Vectors for *Gaia* Photometry

The *Gaia* photometric bands are broad enough to introduce large differences in the color change caused by extinction as a function of the intrinsic stellar color. We calculate extinction vectors by applying the extinction curves of Fitzpatrick (1999) to synthetic stellar spectra from the Phoenix/NEXTGEN grid (BT-Settl version from Allard et al. 2012 with solar abundances from Anders & Grevesse 1989 and $\log g = 4$), and subsequently convolving the reddened spectrum in photon units with the filter transmission curve. Filter curves for *Gaia* DR2 and the spectral templates were obtained from the Spanish Virtual Observatory.

Figure 15 shows the change in *Gaia* G, B_P, and R_P magnitudes for extinctions of $A_V = 1$ and $A_V = 5$ mag and total-to-selective extinction coefficients of $R_V = 3.1$ (adopted in this paper) and 5.5 (see also Table 6). The change in G versus A_V is less for redder stars because most of the G-band photons are red and suffer less from extinction. The change in $B_P - R_P/G$ shows a sharp increase versus extinction A_G for stars cooler than $B_P - R_P = 1.5$, because the R-band photons also dominate the G-band photometry. The $E(B_P - R_P)/A_V$ curve varies much less (within 0.1 mag) for stars with intrinsic colors between $B_P - R_P$ between 0 and 4. For low-mass pre-main sequence stars, the effect of extinction on $B_P - R_P$ versus G is nearly parallel to isochrones, as is also the case with $V - I$ versus V (e.g., Sicilia-Aguilar et al. 2005).
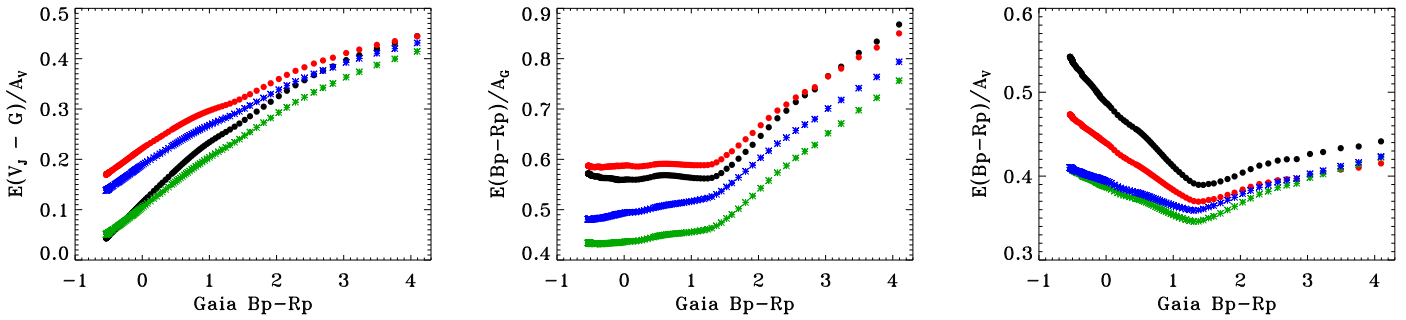
Figure 15. Extinction vectors for *Gaia* A_G/A_V (left), $E(B_P - R_P)/A_G$ (middle), and $E(B_P - R_P)/A_V$ (right) vs. stellar color $B_P - R_P$, for $A_V = 1$ and 5 mag for $R_V = 3.1$ (red and black circles, respectively) and $A_V = 1$ and 5 mag for $R_V = 5.5$ (blue and green asterisks, respectively).

Table 6
Color Changes for $A_V = 1$ mag

T (K)	$B_P - R_P$	$R_V = 3.1$			$R_V = 5.5$		
		$E(V - G)$	$E(V - B_P)$	$E(B_P - R_P)$	$E(V - G)$	$E(V - B_P)$	$E(B_P - R_P)$
2600	4.09	0.44	0.03	0.44	0.41	0.02	0.42
2800	3.49	0.42	0.02	0.43	0.39	0.01	0.41
3000	3.04	0.40	0.02	0.43	0.36	0.01	0.40
3200	2.69	0.38	0.01	0.42	0.34	0.01	0.39
3400	2.42	0.36	0.01	0.42	0.32	0.01	0.38
3600	2.15	0.34	0.01	0.41	0.30	0.00	0.37
3800	1.91	0.31	0.00	0.40	0.28	0.00	0.36
4000	1.70	0.29	0.00	0.39	0.26	0.00	0.36
4200	1.53	0.28	−0.00	0.39	0.25	−0.00	0.35
4400	1.38	0.26	−0.01	0.39	0.23	−0.00	0.35
4500	1.31	0.26	−0.01	0.39	0.23	−0.00	0.35
5000	1.04	0.24	−0.02	0.41	0.21	−0.01	0.35
5500	0.86	0.22	−0.04	0.42	0.19	−0.02	0.36
6000	0.71	0.20	−0.05	0.44	0.18	−0.03	0.37
6500	0.57	0.19	−0.06	0.45	0.16	−0.04	0.37
7000	0.44	0.17	−0.07	0.46	0.15	−0.04	0.37
8000	0.22	0.14	−0.08	0.47	0.13	−0.05	0.38
9000	0.02	0.12	−0.10	0.49	0.11	−0.06	0.39
10,000	−0.07	0.10	−0.11	0.49	0.10	−0.06	0.39
25,000	−0.43	0.06	−0.15	0.53	0.06	−0.09	0.40
33,000	−0.50	0.05	−0.16	0.54	0.05	−0.09	0.41
41,000	−0.51	0.05	−0.16	0.54	0.05	−0.09	0.41
49,000	−0.52	0.05	−0.16	0.54	0.05	−0.09	0.41
57,000	−0.53	0.04	−0.16	0.54	0.05	−0.09	0.41
65,000	−0.54	0.04	−0.16	0.54	0.05	−0.10	0.41

Note. Calculated from synthetic spectra, as described in Appendix A.

Appendix B
The Distance and Extinction to a Sheet of Dust

In this appendix, we describe our code to measure the distance to dust extinction. Dark clouds extinguish emission from background stars, thereby making them fainter and redder. We assume that the cloud is a thin sheet of dust at a single distance, and subsequently simulate stellar populations to estimate the distance d and extinction A_G of the sheet. This idea is similar to distance measurements to dark clouds using *Gaia* DR2 by Yan et al. (2019) and Zucker et al. (2019), *Gaia* DR1 by Voirin et al. (2018), and *Hipparcos* by Whittet et al. (1997), among others, with differences in implementation.

Each simulation includes 500,000 stars that are randomly selected from a parent (or off-cloud) population. If a star is in front of the dust, then the measured stellar parallax, parallax error, and brightness are adopted. If a star is behind the dust,

then the *Gaia* G-band photometry is made fainter by A_G. A new parallax error for this fainter star is adopted by randomly selecting the parallax error for the G-band photometry, based on the distribution of parallax errors in our full data set (Figure 16). All parallaxes, for stars in front of and behind the cloud,[22] are then adjusted by adding the parallax error multiplied by a number randomly selected from a Gaussian distribution.

The parent population is the population that would be present along the line of sight, if extinction were not present. Within the region downloaded for this paper, 28 million stars have $G < 19$ and are located in regions that are not heavily extincted. The stellar density depends on the distance from the

---
[22] Stars with negative parallaxes in the parent sample are assumed to have a parallax equal to 0 mas. This choice does not affect our final results, because the clouds are located within 1 kpc.
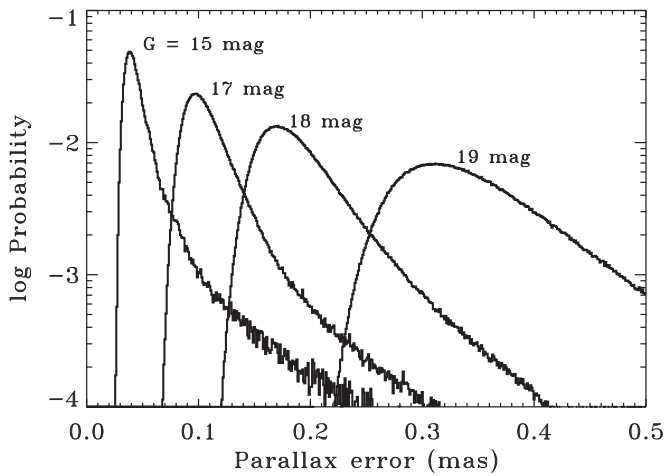
18

Figure 16. The probability distribution of errors for the 140 million stars in the downloaded field, shown here for brightness bands within 0.2 mag of $G = 15$, 17, 18, and 19 mag, in bins of 0.001 mas yr^{-1}. In our simulations, the errors are randomly assigned for the updated brightness with an empirical probability distribution, because the distributions are not well described by Gaussian profiles.

Figure 17. Examples of simulated stellar distributions with $\varpi/\sigma(\varpi) > 20$ vs. distance for an off-cloud population (yellow shaded region), at $A_G = 1$, 2, and 6 mag (red, blue, and purple lines, respectively), with star counts binned to 25 pc.

galactic plane. More stars are located south of the plane, likely because of modest extinction along and just north of the plane. Simulations are therefore run for three different parent populations: stars with the same galactic latitude, stars with the opposite galactic latitude, and stars within some annulus around the region.

The simulated distribution (Figure 17) is then compared to the observed distribution of stars in the line of sight using a two-sided Kolmogorov–Smirnov test. The distribution is scaled to the number of observed stars. Because the clouds in the Serpens star-forming region are located at ~400–500 pc, the comparison is restricted to stars with distances (or simulated distances) less than 1000 pc that are measured (or simulated to be measured) to better than 5% and are brighter (or simulated to be brighter) than $G = 19$ mag. Separate simulations are run for sources with parallaxes measured to better than 20%. The comparison avoids stars with proper motions within 2 mas yr^{-1} of the Serpens clusters. Sources with excess astrometric noise of greater than 2 mas are excluded from the parent sample.

Figure 18 shows results for six different regions. In the simulations, the dropoff in stars versus distance is somewhat gradual, with a cloud distance that is roughly in the center of the dropoff. The width of this dropoff increases as the average $\varpi/\sigma(\varpi)$ of a sample decreases. Even for optically thick clouds, the dropoff can occur at distances closer than expected: stars that are closer than the cloud have errors that can make them appear at larger distances, but there are no stars at larger
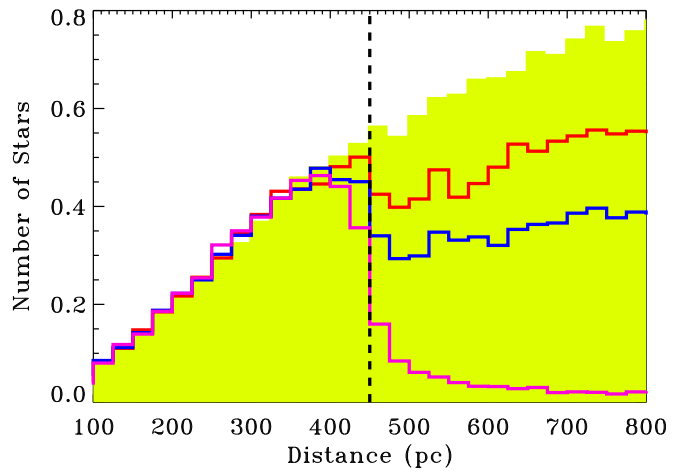
distances that may appear closer than the cloud. Clouds are often patchy, with a range of extinctions; multiple clouds within some region may also be spread across a range of distances. Moreover, the use of samples with $(\varpi/\sigma(\varpi)) > 20$ and > 5 produces different extinctions because they are sensitive to different types of stars. The extinctions measured here are therefore not reliable. Distances obtained from different samples and parallax are always consistent.

This simulation assumes that the errors are accurately evaluated. The parallax error is assumed to be independent of object distance and object color. The excess astrometric noise is also assumed to be independent of distance and color. The parent distribution of *Gaia* sources is assumed to be independent of crowding. The comparison between the simulated and observed distribution is restricted to the distribution of distances in the two samples, so the total number of stars is essentially scaled to match. In principle, this method could be adapted to also test the total stellar population and additional parameters, such as the distribution of brightnesses and colors.

These calculations assume that the extinction occurs in a sheet located at a single distance and with a single extinction. However, molecular clouds are clumpy and may be distributed over some distance. For instance, the Serpens Main cloud extends ~1°, or 7 pc, from south to north, and likely has a similar radial distance. Multiple clouds may be located along the same line of sight, or different lines of sight but within the large beam.
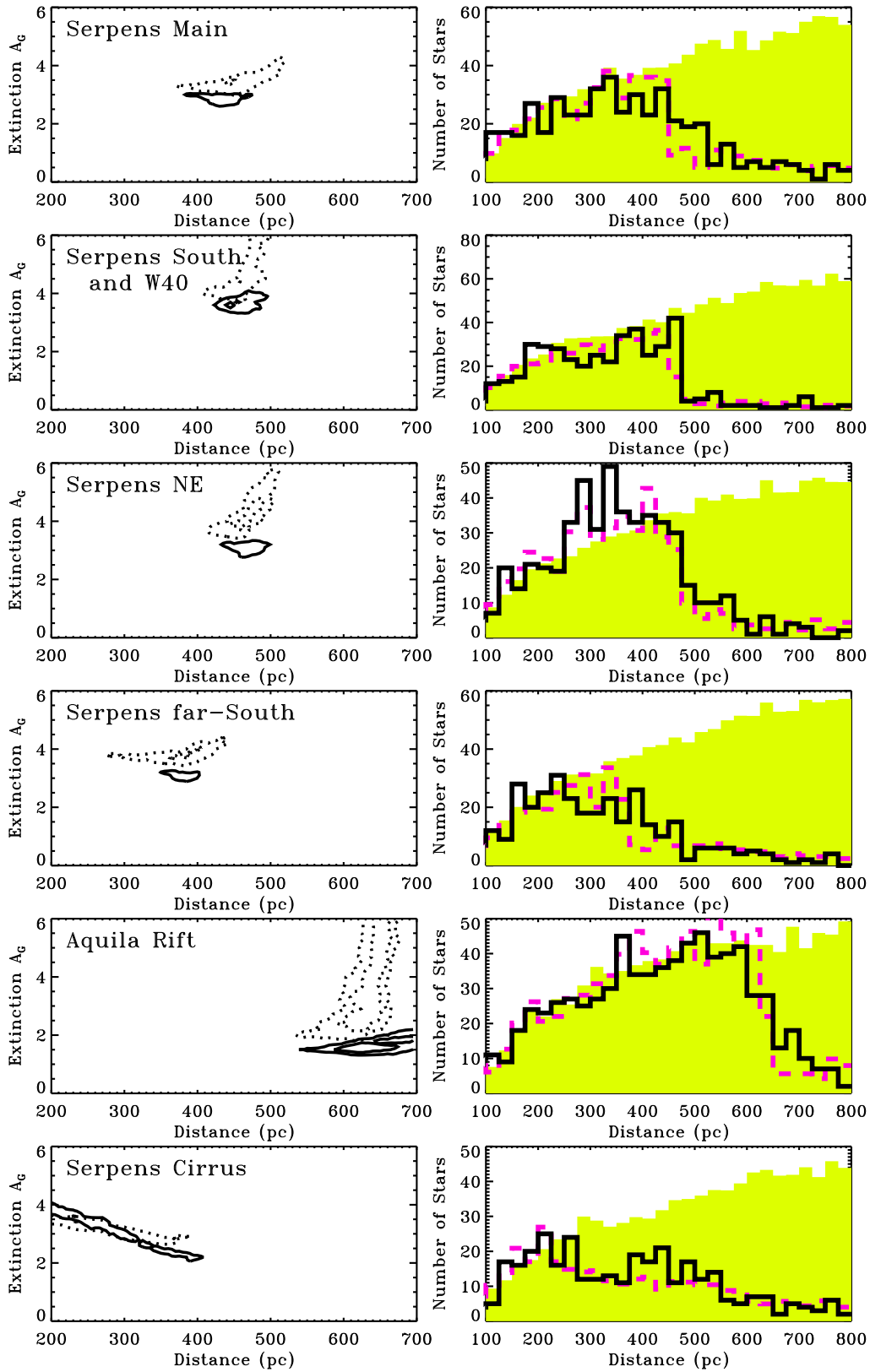
Figure 18. Left: the acceptable distance and extinction parameters from the Kolmogorov–Smirnov (KS) test between a simulated and observed region with confidence contours of 5% and 32%, for stars with parallaxes measured with S/N > 20 (dotted contours) and S/N > 5 (solid contours). The location of the region is provided in Table 3; Aquila Rift is LDN 610, while Serpens Cirrus is near LDN 462. Right: the star counts vs. distance for the region on the left, comparing the observed (black line) and simulated (dashed purple line) populations. The stars in this comparison all have parallaxes measured to S/N > 20. The simulated populated is obtained from a background population (yellow shaded region) with the same absolute galactic latitude at the target region, but south of the galactic plane.

Table 7
High-probability Candidate Members of the Serpens Star-forming Region

R.A.	Decl.	PM(R.A.) (mas yr^{-1})	PM(Decl.) (mas yr^{-1})	ϖ (mas)	$\sigma(\varpi)$ (mas)	G	Bp	R_p	astr.err. (mas)	N_7 (deg)	NPM_7 (mas yr^{-1})	Region
290.06057	11.25336	3.406	−10.253	2.484	0.064	15.501	16.925	14.298	0.25	0.35	0.86	LDN 673
279.73961	0.73944	2.643	−8.491	2.149	0.047	12.928	13.814	11.996	0.12	0.10	0.16	NE
278.88497	0.18238	2.015	−7.629	2.006	0.029	13.324	14.076	12.461	0.00	0.22	0.34	NE
277.50416	0.63222	3.365	−7.908	2.159	0.070	13.448	14.709	12.326	0.40	0.09	0.28	Main
279.06096	−0.34338	1.783	−7.794	1.967	0.030	13.545	14.506	12.558	0.13	0.24	0.29	NE
279.95607	0.51297	2.312	−7.913	2.126	0.025	13.626	14.510	12.697	0.00	0.25	0.15	NE
279.36828	0.39639	3.123	−8.414	2.098	0.328	13.634	14.578	12.659	0.04	0.09	0.35	NE
279.38550	0.70754	3.290	−8.606	2.017	0.034	13.901	14.732	13.004	0.00	0.20	0.46	NE
279.59444	0.61351	2.694	−8.578	2.100	0.046	14.098	15.264	12.998	0.24	0.15	0.19	NE
279.18813	0.88308	3.333	−8.511	2.053	0.036	14.154	15.031	13.225	0.00	0.35	0.57	NE
277.24205	0.29007	2.529	−8.475	2.187	0.041	14.228	15.696	12.998	0.24	0.11	0.36	Main
279.39918	0.31813	2.366	−7.862	2.065	0.046	14.395	15.465	13.348	0.07	0.12	0.21	NE
277.37606	0.70884	2.394	−8.760	2.422	0.034	14.448	15.657	13.370	0.10	0.14	0.29	Main
279.48368	−0.56116	2.753	−8.662	2.098	0.036	14.563	15.545	13.578	0.00	0.17	0.17	NE
277.05635	−0.04708	3.301	−7.615	2.345	0.077	14.635	16.149	13.413	0.29	0.24	0.33	Main
279.81014	0.59363	2.628	−7.859	2.091	0.045	14.650	15.775	13.584	0.19	0.17	0.14	NE
277.26643	0.33920	3.425	−8.124	2.273	0.045	14.751	15.987	13.432	0.23	0.07	0.22	Main
279.26180	−0.42826	2.779	−8.566	2.020	0.037	14.767	15.807	13.761	0.09	0.17	0.14	NE
277.53601	0.97951	3.210	−8.441	2.279	0.050	14.968	16.173	13.853	0.21	0.08	0.21	Main
279.45960	−0.43021	2.802	−8.451	2.200	0.046	14.971	16.069	13.924	0.14	0.09	0.21	NE
279.45040	0.27797	2.074	−7.759	2.116	0.070	15.290	16.444	14.202	0.19	0.17	0.19	NE
277.49322	0.63133	2.970	−8.656	2.198	0.073	15.480	16.962	14.239	0.38	0.09	0.14	Main
285.59253	−5.60571	1.656	−10.015	2.443	0.042	12.783	13.547	11.894	0.00	0.47	1.03	FG Aql

(This table is available in its entirety in machine-readable form.)

Appendix C
A Description of the Online Source List

In an online electronic catalog (see Table 7), we provide a list of all possible Serpens members within 7° of (278, −2), within 3 mas yr^{-1} of a proper motion of (2.5, −8.4) mas yr^{-1}, located at a distance of 320–550 pc, with $\varpi/\sigma(\varpi) > 5$, and with an excess astrometric noise of <2 mas. Beyond the 7° radius, the table also includes several objects near LDN 673, including AS 353A, and the FG Aql group.

The table identifies the highly likely members by listing the region membership, the same targets that are selected for the HR diagrams in Figure 11. Similarly, the likely members of the distributed Serpens star formation are listed as "Distributed." The full table is liberal in including many nonmembers, identified by membership listed as "N/A."

The table also includes nearest neighbor calculations as a way of identifying likely members and small, isolated groups of stars. For this calculation, a parent data set of all stars between 350 and 520 pc with $\varpi/\sigma(\varpi) > 20$ and within 3 mas yr^{-1} of the Serpens proper motion centroid is established. For each star in the full sample, we then calculate the seventh-nearest spatial neighbor within the parent data set. For each star, we also calculate the seventh-nearest proper motion neighbor for stars within a 1° radius within the parent data set. The Serpens members especially stand out as having low seventh-nearest neighbors, with typical distances of <0°4 compared to an average distance of ∼0°7 for field stars. Most members also have a seventh-nearest neighbor in proper motion of <0.5 mas yr^{-1}, while field stars have an average of value of 1.3 mas yr^{-1}. This nearest neighbor analysis alone would produce modest contamination rates, especially away from the main region. A nearest neighbor criterion combined with a photometric selection would have readily identified the LDN 673 group and the FG Aql group as likely members, along with the far southwest extent of Serpens Far-South. In addition, the two stars 2MASS J18435376+0320524 and 2MASS J18430797+0321056 are likely Serpens members and may form a small group.

ORCID iDs

Gregory J. Herczeg (沈雷歌) ● https://orcid.org/0000-0002-7154-6065
Michael A. Kuhn ● https://orcid.org/0000-0002-0631-7514
Jennifer Hatchell ● https://orcid.org/0000-0002-4870-2760
Carlo F. Manara ● https://orcid.org/0000-0003-3562-262X
Doug Johnstone ● https://orcid.org/0000-0002-6773-459X
Michael Dunham ● https://orcid.org/0000-0003-0749-9505
Anupam Bhardwaj ● https://orcid.org/0000-0001-6147-3360
Zhen Yuan (袁珍) ● https://orcid.org/0000-0002-8129-5415

References

Allard, F. 2014, in IAU Symp. 299, Exploring the Formation and Evolution of Planetary Systems, ed. M. Booth, B. C. Matthews, & J. R. Graham (Cambridge: Cambridge Univ. Press), 271
Allard, F., Homeier, D., & Freytag, B. 2012, RSPTA, 370, 2765
Anders, E., & Grevesse, N. 1989, GeCoA, 53, 197
André, P., Men'shchikov, A., Bontemps, S., et al. 2010, A&A, 518, L102
Arenou, F., Luri, X., Babusiaux, C., et al. 2018, A&A, 616, A17
Beccari, G., Boffin, H. M. J., Jerabkova, T., et al. 2018, MNRAS, 481, L11
Beccari, G., Petr-Gotzens, M. G., Boffin, H. M. J., et al. 2017, A&A, 604, A22
Blaauw, A. 1956, ApJ, 123, 408
Bontemps, S., André, P., Könyves, V., et al. 2010, A&A, 518, L85
Bressan, A., Marigo, P., Girardi, L., et al. 2012, MNRAS, 427, 127
Cambrésy, L. 1999, A&A, 345, 965
Cantat-Gaudin, T., Jordi, C., Vallenari, A., et al. 2018, A&A, 618, A93
Cantat-Gaudin, T., Jordi, C., Wright, N. J., et al. 2019, A&A, 626, A17

Capitanio, L., Lallement, R., Vergely, J. L., Elyajouri, M., & Monreal-Ibero, A. 2017, A&A, 606, A65
Cunningham, A. J., Krumholz, M. R., McKee, C. F., & Klein, R. I. 2018, MNRAS, 476, 771
Cutri, R. M., Skrutskie, M. F., van Dyk, S., et al. 2003, The IRSA 2MASS All-Sky Point Source Catalog, NASA/IPAC Infrared Science Archive, http://irsa.ipac.caltech.edu/applications/Gator/
Dame, T. M., Hartmann, D., & Thaddeus, P. 2001, ApJ, 547, 792
Dame, T. M., & Thaddeus, P. 1985, ApJ, 297, 751
Damiani, F., Prisinzano, L., Pillitteri, I., Micela, G., & Sciortino, S. 2019, A&A, 623, A112
Davis, C. J., Matthews, H. E., Ray, T. P., Dent, W. R. F., & Richer, J. S. 1999, MNRAS, 309, 141
de Zeeuw, P. T., Hoogerwerf, R., de Bruijne, J. H. J., Brown, A. G. A., & Blaauw, A. 1999, AJ, 117, 354
Dias, W. S., Alessi, B. S., Moitinho, A., & Lépine, J. R. D. 2002, A&A, 389, 871
Dobashi, K. 2011, PASJ, 63, S1
Duarte-Cabral, A., Fuller, G. A., Peretto, N., et al. 2010, A&A, 519, A27
Dunham, M. M., Allen, L. E., Evans, N. J., II, et al. 2015, ApJS, 220, 11
Dzib, S. A., Loinard, L., Ortiz-León, G. N., Rodríguez, L. F., & Galli, P. A. B. 2018, ApJ, 867, 151
Eiroa, C., & Casali, M. M. 1992, A&A, 262, 468
Eiroa, C., Djupvik, A. A., & Casali, M. M. 2008, in Handbook of Star Forming Regions, Volume II: The Southern Sky, Vol. 5, ed. B. Reipurth (San Francisco, CA: ASP), 693
Erickson, K. L., Wilking, B. A., Meyer, M. R., et al. 2015, AJ, 149, 103
Evans, D. W., Riello, M., De Angeli, F., et al. 2018, A&A, 616, A4
Fang, M., Pascucci, I., Edwards, S., et al. 2018, ApJ, 868, 28
Fang, M., van Boekel, R., Bouwman, J., et al. 2013, A&A, 549, A15
Fitzpatrick, E. L. 1999, PASP, 111, 63
Gaia Collaboration, Brown, A. G. A., Vallenari, A., et al. 2018, A&A, 616, A1
Gaia Collaboration, Prusti, T., de Bruijne, J. H. J., et al. 2016, A&A, 595, A1
Gehman, C. S., Adams, F. C., & Watkins, R. 1996, ApJ, 472, 673
Getman, K. V., Broos, P. S., Kuhn, M. A., et al. 2017, ApJS, 229, 28
Getman, K. V., Feigelson, E. D., & Kuhn, M. A. 2014, ApJ, 787, 109
Getman, K. V., Feigelson, E. D., Kuhn, M. A., et al. 2018, MNRAS, 476, 1213
Giardino, G., Favata, F., Micela, G., Sciortino, S., & Winston, E. 2007, A&A, 463, 275
Gorlova, N., Steinhauer, A., & Lada, E. 2010, ApJ, 716, 634
Green, G. M., Schlafly, E. F., Finkbeiner, D., et al. 2018, MNRAS, 478, 651
Green, G. M., Schlafly, E. F., Finkbeiner, D. P., et al. 2015, ApJ, 810, 25
Gutermuth, R. A., Bourke, T. L., Allen, L. E., et al. 2008, ApJL, 673, L151
Haisch, K. E., Jr., Lada, E. A., & Lada, C. J. 2001, ApJL, 553, L153
Heiderman, A., & Evans, N. J., II 2015, ApJ, 806, 231
Herbig, G. H., & Bell, K. R. 1988, Third Catalog of Emission-Line Stars of the Orion Population (Santa Cruz, CA: Lick Observatory)
Hernández, J., Hartmann, L., Calvet, N., et al. 2008, ApJ, 686, 1195
Ibáñez-Mejía, J. C., Mac Low, M.-M., Klessen, R. S., & Baczynski, C. 2017, ApJ, 850, 62
Jose, J., Kim, J. S., Herczeg, G. J., et al. 2016, ApJ, 822, 49
Kirk, H., Pineda, J. E., Johnstone, D., & Goodman, A. 2010, ApJ, 723, 457
Könyves, V., André, P., Men'shchikov, A., et al. 2015, A&A, 584, A91
Kounkel, M., Covey, K., Suárez, G., et al. 2018, AJ, 156, 84
Kuhn, M. A., Feigelson, E. D., Getman, K. V., et al. 2014, ApJ, 787, 107
Kuhn, M. A., Getman, K. V., Feigelson, E. D., et al. 2010, ApJ, 725, 2485
Kuhn, M. A., Hillenbrand, L. A., Sills, A., Feigelson, E. D., & Getman, K. V. 2019, ApJ, 870, 32
Kuhn, M. A., Povich, M. S., Luhman, K. L., et al. 2013, ApJS, 209, 29
Lallement, R., Vergely, J.-L., Valette, B., et al. 2014, A&A, 561, A91
Lee, J.-E., Lee, S., Baek, G., et al. 2019, NatAs, 3, 314
Leung, H. W., & Bovy, J. 2019, arXiv:1902.08634
Lindegren, L., Hernández, J., Bombrun, A., et al. 2018, A&A, 616, A2
Lodieu, N., Bouvier, J., James, D. J., et al. 2006, A&A, 450, 147
Luhman, K. L. 2018, AJ, 156, 271

Luri, X., Brown, A. G. A., Sarro, L. M., et al. 2018, A&A, 616, A9
Lynds, B. T. 1962, ApJS, 7, 1
Mairs, S., Johnstone, D., Kirk, H., et al. 2016, MNRAS, 461, 4022
Mallick, K. K., Kumar, M. S. N., Ojha, D. K., et al. 2013, ApJ, 779, 113
Mamajek, E. E. 2009, in AIP Conf. Proc. 1158, Exoplanets and Disks: Their Formation and Diversity, ed. T. Usuda, M. Tamura, & M. Ishii (Melville, NY: AIP), 3
Manara, C. F., Prusti, T., Comeron, F., et al. 2018, A&A, 615, L1
Marigo, P., Girardi, L., Bressan, A., et al. 2017, ApJ, 835, 77
Meyer, M. R., Calvet, N., & Hillenbrand, L. A. 1997, AJ, 114, 288
Mundt, R., Stocke, J., & Stockman, H. S. 1983, ApJL, 265, L71
Nakamura, F., Dobashi, K., Shimoikura, T., Tanaka, T., & Onishi, T. 2017, ApJ, 837, 154
Nakamura, F., Sugitani, K., Shimajiri, Y., et al. 2011, ApJ, 737, 56
Ortiz-León, G. N., Dzib, S. A., Kounkel, M. A., et al. 2017, ApJ, 834, 143
Ortiz-León, G. N., Loinard, L., Dzib, S. A., et al. 2018, ApJL, 869, L33
Pirogov, L., Ojha, D. K., Thomasson, M., Wu, Y.-F., & Zinchenko, I. 2013, MNRAS, 436, 3186
Povich, M. S., Kuhn, M. A., Getman, K. V., et al. 2013, ApJS, 209, 31
Prato, L., Rice, E. L., & Dame, T. M. 2008, in Handbook of Star Forming Regions, Volume I: The Northern Sky, Vol. 4, ed. B. Reipurth (San Francisco, CA: ASP), 18
Preibisch, T., & Zinnecker, H. 1999, AJ, 117, 2381
Racine, R. 1968, AJ, 73, 233
Rice, E. L., Prato, L., & McLean, I. S. 2006, ApJ, 647, 432
Richert, A. J. W., Getman, K. V., Feigelson, E. D., et al. 2018, MNRAS, 477, 5191
Roccatagliata, V., Sacco, G. G., Franciosini, E., & Randich, S. 2018, A&A, 617, L4
Rodney, S. A., & Reipurth, B. 2008, in Handbook of Star Forming Regions, Volume II: The Southern Sky, Vol. 5, ed. B. Reipurth (San Francisco, CA: ASP), 683
Rumble, D., Hatchell, J., Gutermuth, R. A., et al. 2015, MNRAS, 448, 1551
Sharpless, S. 1959, ApJS, 4, 257
Shimoikura, T., Dobashi, K., Nakamura, F., et al. 2015, ApJ, 806, 201
Shimoikura, T., Dobashi, K., Nakamura, F., Shimajiri, Y., & Sugitani, K. 2018, PASJ, in press (doi:10.1093/pasj/psy115)
Shuping, R. Y., Vacca, W. D., Kassis, M., & Yu, K. C. 2012, AJ, 144, 116
Sicilia-Aguilar, A., Hartmann, L. W., Hernández, J., Briceño, C., & Calvet, N. 2005, AJ, 130, 188
Siess, L., Dufour, E., & Forestini, M. 2000, A&A, 358, 593
Slesnick, C. L., Hillenbrand, L. A., & Carpenter, J. M. 2008, ApJ, 688, 377
Smith, J., Bentley, A., Castelaz, M., et al. 1985, ApJ, 291, 571
Soderblom, D. R., Hillenbrand, L. A., Jeffries, R. D., Mamajek, E. E., & Naylor, T. 2014, in Protostars and Planets VI, ed. H. Beuther et al. (Tucson, AZ: Univ. Arizona Press), 219
Straižys, V., Černis, K., & Bartašiūtė, S. 1996, BaltA, 5, 125
Straižys, V., Černis, K., & Bartašiūtė, S. 2003, A&A, 405, 585
Strom, S. E., Grasdalen, G. L., & Strom, K. M. 1974, ApJ, 191, 111
Stutz, A. M., & Gould, A. 2016, A&A, 590, A2
Tafalla, M., Myers, P. C., Mardones, D., & Bachiller, R. 2000, A&A, 359, 967
Townsley, L. K., Broos, P. S., Garmire, G. P., et al. 2014, ApJS, 213, 1
Vázquez-Semadeni, E., Zamora-Avilés, M., Galván-Madrid, R., & Forbrich, J. 2018, MNRAS, 479, 3254
Voirin, J., Manara, C. F., & Prusti, T. 2018, A&A, 610, A64
Westerhout, G. 1958, BAN, 14, 215
Whittet, D. C. B., Prusti, T., Franco, G. A. P., et al. 1997, A&A, 327, 1194
Winston, E., Megeath, S. T., Wolk, S. J., et al. 2010, AJ, 140, 266
Winston, E., Wolk, S. J., Gutermuth, R., & Bourke, T. L. 2018, AJ, 155, 241
Yan, Q.-Z., Zhang, B., Xu, Y., et al. 2019, A&A, 624, A6
Zari, E., Hashemi, H., Brown, A. G. A., Jardine, K., & de Zeeuw, P. T. 2018, A&A, 620, A172
Zeilik, M., II, & Lada, C. J. 1978, ApJ, 222, 896
Zhu, L., Wu, Y.-F., & Wei, Y. 2006, ChJAA, 6, 61
Zucker, C., Speagle, J. S., Schlafly, E. F., et al. 2019, arXiv:1902.01425